FABRICATION AND EVALUATION OF

GaAlAs CSP LASERS

THE PROCESSING AND EVALUATION OF LONG

LIVED GaAlAs CHANNELED SUBSTRATE

PLANAR LASERS

BY

CHRISTOPHER MICHAEL LOOK, B.Sc.

A Thesis

Submitted to the School of Graduate Studies

in Partial Fulfillment of the Requirements

for the Degree

Master of Engineering

McMaster University

September 1980

MASTER OF ENGINEERING (1980)   McMASTER UNIVERSITY
(Engineering Physics)   Hamilton, Ontario

TITLE: The Processing and Evaluation of Long Lived GaAlAs
           Channeled Substrate Planar Lasers

AUTHOR: Christopher Michael Look, B.Sc. (Simon Fraser University)

SUPERVISOR: Dr. A.J. SpringThorpe

NUMBER OF PAGES: iv, 43.

ABSTRACT

The theory of operation and advantages of a channeled substrate planar (CSP) laser is described. The processing of such devices utilizing 5 μm wide proton bombardment defined current stripes is detailed. The optical and electrical characteristics of the resultant devices is presented. The lasers had pulsed, room temperature thresholds averaging 90mA, lased predominantly in a single longitudinal mode and were kink-free to power levels in excess of 6mW. Accelerated aging yielded an "activation energy" for the degradation process of 0.7eV which allowed for a predicted useful lifetime of 5 x 10^4 hours for these lasers.

ACKNOWLEDGEMENTS

INTRODUCTION

The development of low-loss optical fibers has already resulted in a rapid proliferation of optical communication systems taking advantage of the RFI/EMI noise immunity, security and large bandwidths offered. GaAs 'Burrus'-type[1] light-emitting diodes (LED's) with a peak emission wavelength of 0.84 µm are frequently used as the optical source in such systems because of their demonstrated long life, high radiance and good linearity. However, in order to take full advantage of the potential bandwidth of optical fibers, a light source with a much narrower emission linewidth must be used to reduce the effects of material dispersion. Typical LED's have linewidths of ~450 Å full width at half maximum (FWHM) which results in a pulse spreading of 1-2 ns/km for typical low-loss graded index optical fibers[2]. $Ga_{1-x}Al_xAs$ double hetero-structure (DH) lasers have linewidths $\le$ 20 Å (FWHM), and can be even $\le$ 1 Å if they lase in a single longitudinal mode. This can reduce the pulse spreading to $\le$ 0.1 ns/km and thus increase the amount of information which can be transmitted through a given length of fiber.

The intense coherent optical fields in the laser cavity can shorten the injected carrier lifetime to less than the spontaneous lifetime (τ_{spont} ~2ns) and make possible Gbit modulation rates. In addition, the high degree of directionality of laser emission results in high coupling efficiencies into optical fibers. Furthermore laser diodes are the only practical solid state devices capable of coupling sufficient power into single mode step-index fibers to justify their use[3].

The primary reasons for lasers not being used more extensively in the field are:

   i. high cost,
  ii. relatively rapid degradation,
 iii. large current requirements,
  iv. sensitivity of output power to temperature variations and,
   v. gross non-linearities in the light output vs current (L-I)

While the cost of $Ga_{1-x}Al_xAs$ lasers can be expected to drop as the quantity fabricated increases, much research effort must yet be made to isolate the causes and minimize the effects of the other problems. The primary goal of this project was to increase the linearity of the laser. As a side effect, improvements in thresholds and lifetimes could be expected.

Conventional stripe geometry lasers are made with narrow ($\leq$ 20 μm) contact stripes in order to reduce the current threshold and prevent multi-filament operation.[4] Improvements in fiber coupling efficiency also results from the use of narrow stripes. Unfortunately, such lasers frequently show gross non-linearities in their L-I characteristics. It is common for the external efficiency to be negative over appreciable current ranges and even for the light output to be increasing at one facet while decreasing at the other facet of the same laser[5] (fig. 1). Such "kinks" are obviously undesirable for analogue transmission. Additionally, light output stabilization, linearization or temperature compensation schemes based on feeding back a portion of the optical output will fail to work at such kinks. The light output also frequently exhibits a directional shift at the kink which can result in poor coupling into fibers[6]. Furthermore, modulation at microwave frequencies is not possible due to spontaneous pulsations (at 0.2-2 GHz rates) in the light output when the laser is operated at current levels near a kink[7].

Kinks have been investigated theoretically by Chinone[8] and were shown to arise from a local saturation in the gain profile as a result of the stimulated recombination of carriers directly beneath the center of the contact stripe. In conventional planar stripe geometry double-heterostructure lasers, the active region width and dielectric steps are well defined by the material discontinuities in the x-direction (fig. 2), resulting in discrete allowed mode structures in this direction. In the other transverse direction, the only dielectric variation is that due to the injected carrier density. The index variation in this plane is very nearly parabolic resulting in parabolic wavefronts and far field patterns which correspond closely to Hermite-Gaussian modes[9]. In the absence

of strong dielectric confinement the predominant transverse mode control mechanism is spatial variation of the carrier inversion (i.e. high optical gain regions). The lasing threshold condition for any given mode, m, is[10]

$$\Gamma g(E,m) = \Gamma \alpha_{fc} + (1-\Gamma)\alpha_{fc, x} + \alpha_{scatt,m} + \alpha_{coupling, m} + \frac{1}{L} \ln R_m$$

(variables defined in Fig. 9). As the transverse mode number increases the maxima of intensity move further away from the center of the stripe, see fig. 3. At low injection levels, low order Hermite-Gaussian modes reach threshold first because the gain is a maximum directly beneath the center of the stripe. At higher current levels, the injected carriers near the center of the stripe recombine so rapidly, as a result of the strong stimulated recombination, that the injected carrier profile, and hence the gain profile, become flattened (fig. 4). As a result of the reduced gain in this region, the light output begins to saturate, which manifests itself as a rounding off of the L-I characteristic. At sufficiently high current levels, the gain profile has spread out so far laterally that higher order modes are able to pick up enough gain to reach threshold and, as the gain is not yet saturated for these modes, the L-I characteristic again increases. If there is any asymmetry in the cavity such as local variations in the current density, internal quantum efficiency, or compositional/geometrical variations, then a shift in the direction of the output beam may occur. Such a shift would not be expected for a simple Fabry-Perot structure, but the strong gain guiding of the modes permits small angular variations (~ 2°) from the mirror normal without appreciable loss[11].

Chinone concluded that kinks would occur regardless of crystal quality and that in order to keep higher order transverse modes from lasing it would be necessary to employ either strip widths under ~8 µm (so that the lateral extent of the inverted carrier population would not be great enough to provide the threshold gain for higher order modes) or to use a cavity structure in which the gain profile would not be determined solely by the lateral diffusion of carriers away from the stripe center.

There have been a number of device geometries proposed to stabilize the transverse mode structure. Among them are the transverse junction stripe (TJS)[13], misaligned stripe[14], buried heterostructure (BH)[15], channeled substrate planar (CSP)[16] and buried channeled substrate lasers[17]. The CSP structure was chosen for this investigation because it should posess excellent mode control and still be relatively easy to fabricate with our existing technology.

Theory

In the CSP laser, a narrow groove is made in the GaAs substrate prior to LPE growth (fig. 5). A thin first confining layer of n-type $Ga_{1-x}Al_xAs$ is then grown which fills in the channel and allows successive layers to be essentially planar. Modes propagating outside the channel in region B, are not wholly confined to the active layer but spread out and have evanescent tails reaching into the GaAs substrate. As the substrate is unpumped, and has the peak of its absorption spectrum at approximately the lasing wavelength[18], the radiation will be strongly absorbed resulting in high modal losses. In the channel region A, the depth of the channel is sufficient to ensure that the evanescent wave sees only the larger band gap, and hence transparent, $Ga_{.7}Al_{.3}As$. Modes which are confined to the channel region will have a much lower modal loss than higher order ones and will reach threshold much sooner. The mechanism for mode control is seen to be built-in loss-guiding, in addition to carrier diffusion defined gain-guiding as distinct from just gain guiding, which is the lateral mode control mechanism in standard and misaligned stripe lasers.

The extra loss can be incorporated in the cavity equations as a change in the complex index of refraction seen by the wave. The degree of mode confinement will be determined in part by the index difference between the two regions $\Delta \tilde{n} = \Delta n + i \, \Delta \alpha / 2 k_0$; where $\Delta n = n_A - n_B$, $\Delta \alpha = \alpha_B - \alpha_A$ and k_0 is the wavenumber. The n_i and α_k are "effective" index and losses, respectively, because regions A and B are not uniform and contain material discontinuities characterized by the active layer thickness (d) and the first confining layer thickness (t).

Theoretical calculations relating $\Delta \tilde{n}$ to t and d have been carried out by Aiki et al[19] (fig. 6). In order that the structure provide strong, stable mode guiding, $|\Delta n|$ must be greater than any index change resulting from the injected carriers. As these effects are estimated[20] to be $|\Delta n_{carriers}| \sim 10^{-3}$, fig. 6, this imposes severe restrictions on t and d. Even dimensions as small as t = 0.5 μm coupled with d = 0.3 μm will only result in $|\Delta \tilde{n}| \approx 2 \times 10^{-4}$ which is insufficient to override the current gain-guiding.

As with conventional DH lasers, thin active layers result in lower thresholds and a narrower emission perpendicular to the plane of the junction. The sensitivity of the mode control on d for a CSP laser is related to the increased evanescent tails of the mode extending away from the active layer into the confining layers as d decreases. A thinner active region results in a larger fraction of the mode (1- Γ) propagating in the confining layers. Thus for a CSP laser, the potential for mode control is improved. Very thin active layers can be difficult to achieve in practice because of the danger of incomplete wetting by the growth solution on the first confining layer which results is partial or total pinch-off of the active layer. A thicker than optimal active layer can be compensated for by making t smaller, thus enabling the evanescent wave to still reach the absorbing substrate.

The choice of channel width is necessarily restricted, because if it is too wide there will be no significant mode selection (fig. 6c). A very narrow channel (≤ 5 μm) will raise the threshold for even the fundamental mode. Channel widths of 5-8 μm appear optimal.

DEVICE FABRICATION

Substrate grade n-type GaAs (nominal dislocation density = $4x10^3cm^{-2}$, N_D = $5x10^{17}cm^{-3}$) was lightly polished on one of its (100) faces and then had 3 mil openings photo-engraved on it. A preferential etch (1% Bromine in methanol) was used to identify the crystal face having the $[01\bar{1}]$ direction running parallel to its long side (fig. 7). After this identification was made, the chosen side was given a final chemical/mechanical polish with Br_2-methanol. Five micron wide stripes were laid down on this side using conventional photoengraving techniques. It was necessary to have these stripes aligned with $[01\bar{1}]$ so that the channels would have the V-shaped walls defined by its slow etching {111} planes fig. 8. The channels were nominally 1.2 μm deep and 7.5 μm wide at the shoulders. They were wider than the photoresist mask due to undercutting by the preferrential etch.

The crystals were grown by liquid phase expitaxy using the standard carbon slider technique. The channels on the substrate were aligned with the direction of push to ensure good filling of the channels by the growth solution. Four layers (fig. 9) were then grown consecutively on the prepared substrate at the relatively low growth temperature of 760°C with a cooling rate of 0.25°C/minute. The low growth temperature was necessary in order to prevent etching of the channel by the first confining layer growth solution.

The active layer was doped with germanium to give an acceptor density of ~$5x10^{17}cm^{-3}$. A small amount of aluminum (6%) was also added to increase the emission energy to enable a more favorable match to the minima in optical fibers absorption. It also reduced the lattice mismatch between the active layer and the confining layers. However, perhaps the most important reason for the addition of small amounts of Al to the active layer is the observation that the lifetime of such lasers is significantly better than for lasers with pure GaAs active layers (fig. 10). This improvement is believed due to the presence of aluminum which acts

as a getter for oxygen and prevents it incorporation into the crystal.
Oxygen is thought to be associated with dark-line defect degradation
mechanisms[4].

The aluminum concentration in the confining layers was ~34% for two
reasons. It provides,

1) a sufficient energy step ($\Delta E = 0.37eV$) to confine the injected
   carriers, and,

2) an index change ($\Delta n = 0.17$) for optical confinement.

The top capping layer had a reduced bandgap compared to the second
confining layer to facilitate an ohmic contact to the final device.

Lasers were fabricated using both proton-bombardment and oxide stripe
device technologies. Oxide stripe lasers had their contacts made by first
depositing silicon dioxide on the wafer by a chemical vapour deposition
(CVD) process. Five micron stripes aligned over the channels were opened
up through a photoresist mask using buffered hydroflouric acid to etch
away the SiO_2. Zinc was diffused ~0.2 μm into the top
$p-Ga_{.93}Al_{.07}As$ contact through the SiO_2 mask to degenerately
dope (~$10^{19}cm^{-3}$) the surface in order to provide a low resistance
ohmic contact.

Proton-bombarded slices were zinc diffused over the whole wafer and
then had 2 μm thick x 5 μm wide gold stripes plated over the channels.
The wafers were then irradiated with 300 keV protons which penetrated into
the crystal a distance of ~1.8 μm except directly over the channel where
the plated gold stripes protected the region from damage. As the protons
were slowed down by scattering from the crystal's atoms, low level carrier
traps were created which caused the resistance in the damaged regions to
increase. The depth of penetration of the proton distribution was chosen
so that the active region was not damaged. This was because the induced
damage would absorb optical radiation (thus raising the lasing threshold)
as well as having possible deleterious effect on device lifetimes.
Subsequent processing steps were chosen with care so as not to anneal out
the proton induced damage.

The p-side contact metallization was made by evaporating a chrome-gold layer over the entire surface followed by plating gold heat sinks over the channels. Both varieties of lasers were mechanically lapped down to 100 μm in thickness and had germanium/gold eutectic contacts evaporated on the n-GaAs substrate. Windows were opened up in this contact, over the channel, which allows the stripe region to be viewed through the GaAs substrate by means of an infra-red microscope (fig. 11). At the same time that the windows were photoengraved, each laser was numbered, which enabled the subsequent determination of its position in the grown slice.

RESULTS

Scanning electron microscope pictures of the laser chips (fig. 12) show that the channel had filled in well resulting in no observable modulation of the active layer thickness. The cleaved edge of the crystal was treated with a selective etch to delineate the various layers. Tapered regions which occur at a boundary between two different compositional regions cannot be unambiguously ascribed to one region or the other. With this limitation, the active layer thickness was $0.1 - 0.2$ μm thick, which was the designed value. The first confining layer was ~ 1.2 μm thick however and was too thick for effective mode control. Complications arose in attempting to grow very thin (< 1.0 μm) first confining layers because not only is the growth rate a non-linear function of time on a smooth substrate, but there is some indication of an enhancement of the growth rate over a fairly wide area in the vicinity of the groove (fig. 13). This is believed due to the easy initial growth on the exposed planes in the channel. Figure 12 also shows evidence of melt-back of the substrate before growth. This may be due to under-saturation of the growth solution since other wafers showed the channel inclination to be closer to the $54°44'$ expected of the {111} slow etch planes.

The pulsed thresholds were determined before bonding by mounting the laser chip in a temporary pressure contact package and visually observing the sharp turn-on of the far-field interference pattern characteristic of lasing threshold. The low thresholds (summarized in fig. 14) can be attributed to the thin active layer. The threshold can be expected to decrease almost linearly with active layer thickness (for $d \leqslant \lambda/n_o =$ 0.23 μm) because of the smaller confinement volume it represents. For $d \leqslant 0.23$ μm, the decrease in the optical mode confinement factor Γ causes a rounding off of the threshold to minimum at $d \approx 0.08$ μm and a sharp increase thereafter.

The lowest threshold observed was 65 mA which corresponded to a threshold current density $J_{th} = 3210$ A/cm^2. The averages for the oxide stripe and proton bombarded lasers were 120 mA ($J_{th} = 5930$ A/cm^2) and 100 mA ($J_{th} = 4940$ A/cm^2) respectively. These

values are a factor of 3x higher than the calculated value of 1725 A/cm^2 (fig. 9) for a broad area device. The primary reason for the difference is that the theoretical J_{th} was calculated for a broad area laser and neglected both current spreading from the contact to the active layer and the lateral diffusion of carriers confined to the active region. The observed factor of 2-4 times the broad area thresholds seems consistent with data presented by Casey and Panish (fig. 15). Scatter in the threshold values within a given wafer was due in large part to unwanted plating through the photoresist mask which allowed current flow in small areas which had escaped bombardment. This problem will be eliminated in future crystals due to refinements in substrate preparation, which allows for a smoother as-grown surface. Additional current confinement using oxide stripe contacts in combination with proton bombardment are also planned.

The pulsed efficiencies were determined while still in the temporary packages by pulsing the laser (1 μs pulses at 1 kHz repetetion rate) and monitoring the steady state light output with a calibrated solar cell. No heating was observed at this rep rate for pulse lengths less than 10 μs and the slow response of the solar cell averaged out any pulsations in the light output. External differential efficiencies (η_{ext}) as high as 0.44 W/A (=> differential power efficiencies = 0.29, single facet) were observed, with 0.4 W/A being typical (fig. 16). These values agreed well with the calculated η_{ext} = 0.29 (fig. 9) on the assumption that the internal quantum efficiency (η_i) was 0.7, a value frequently reported by other workers[21].

The outputs appeared strictly linear up to power levels of 4-5 mW before deviating from straight lines. The values of current thresholds calculated from these plots were consistant with the visually determined values.

For D.C. operation, good heat sinking is essential and, while the XO-72 header is easy to bond to, a significant fraction (~1/3) of the light scatters off the header. This scattering reduced the bonded measured efficiencies and had the effect of making kinks appear at lower measured output powers.

The D.C. thresholds were ~5 mA higher than pulsed ones (fig. 17) agreeing with subsequent data which suggest that the thermal resistance of the bonded device was as high as 50°C/Watt. For such values of thermal resistance, a D.C. current of 90 mA would result in a temperature rise at the active region of ~8°C.

Pulsed threshold vs temperature measurements (fig. 18) could be reasonably expressed as $I_{th}(T°K) = 9.2e^{T/138}$ for $T \leq 345°K$ (72°C). The increase in temperature variation above ~350°K is believed due to a decrease in the injection efficiency resulting from a larger percentage of thermally excited carriers being able to surmount the confining heterojunction potentials. A deviation from this simple exponential relation is not unexpected, as the expression is empirical and has no theoretical basis. The primary cause for the temperature dependance is the need to inject additional carriers to sustain a given population inversion (gain) as the temperature increases. The temperature dependance is not particularly strong when compared with lasers fabricated in other labs[22], however. In combination with a thermal resistance of 50°C/W, it is expected that the D.C. threshold will increase by 5 mA over the 90 mA pulsed threshold.

Both pulsed and D.C. spectra (fig. 19) show that below and just above threshold the output consisted of a number of Fabry-Perot modes. (The intensity envelope for the modes outlines the gain curve). As the pumping rate was increased to ~1.2 I_{th}, the laser oscillated predominantly in a single longitudinal mode. The frequency of the lasing mode was observed to shift (fig. 20) to shorter wavelengths as the pulsed current was increased. This shift can be attributed to a filling in of the band tails caused by the high doping levels. As the excitation rate increased, injected carriers were restricted, by the Pauli exclusion principal, to occupy ever higher energy states. This increased the effective Fermi level seperation and allowed higher frequencies to satisfy[23] $h\nu_L < E_{fc} - E_{fv}$, (where ν_L = lasing frequency, and E_{fc}, E_{fv} are the quasi-Fermi levels for electrons and holes, respectively).

When operated under D.C. conditions, similar spectral behavior was observed except that the wavelength of the single lasing longitudial mode was 20-30 Å longer. The internally dissipated power raised the junction temperature causing the lattice to expand and the energy gap to decrease, thus allowing lower energy frequencies to satisfy $h\nu_L > E_{gap}$. For pure GaAs, the energy gap has been found to vary as $Eg = 1.519 - (5.405 \times 10^{-4} \cdot T^2/(204+T))$ (eV)[24]. A rise in temperature of 7°K above room temperature (293°K), decreases the energy gap by 0.0003 eV corresponding to an increase in wavelength of 19 Å. This suggests that the thermal resistance of the device could be <R> = 45°C/W. However, this value is only approximate, due to reported hysteresis in the lasing wavelength with temperature[25]. Numerical calculations on similar proton-bombarded structures by Joyce and Dixon[26] gave values of thermal resistance <R> of 20.6°C/W for a laser of stripe width 12 μm and cavity length 375 μm. Approximate extensions to the present CSP geometry could be made using a chart included in their paper which showed the effect of a factor of two variation in critical dimensions. According to their results, our shorter cavity length (250 μm), smaller active region width (7.5 μm) and thicker second confining region (1.5 μm) all act to increase the <R> to 40.1°C/W. It would not seem likely that the thermal resistance could be decreased much beyond the experimentally observed values without undesirable changes in device geometry.

The longitudinal mode spacing was $\Delta\Gamma = 3.7 \pm 0.1$ Å which corresponds to a cavity length of 260 ± 10 m assuming Fabry–Perot spacings

$$(\Delta\lambda = \lambda^2/2Ln(1 - \frac{\lambda}{n}\frac{dn}{d\lambda})$$

n = index of refraction of GaAs). The width of the mode was limited by the resolution of the spectrometer to an upper limit of ≤1.5 Å. If the FWHM is taken to be 1 Å then the frequency spread is only $\Delta\dot{\nu} = \frac{c\Delta\lambda}{\lambda^2}$ = 44 GHz, similar to the values obtained by Aiki et al[19].

It is interesting to note that the longitudinal modes do not lase in turn but jump over some to lase in selected ones (fig. 20). This behavior can be interpreted in terms of a hysteresis effect proposed in a later section.

A CCD sensing array was used to record the far-field radiation patterns. In the direction perpendicular to the junction plane, the thin active region and the large dielectric step combined to restrict the optical field distribution to its lowest order mode at all current levels used (up to $2I_{th}$ pulsed). As shown in fig. 21(d), the pattern was symmetrical and had a FWHM = 46 $\pm$ 2°. Numerical calculations (44) using the nominal layer thicknesses and compositional steps result in a predicted FWHM = 48°.

In general, mode patterns in the direction parallel to the junction plane did not indicate lowest order transverse mode operation only. Instead, (fig. 21a,b) the patterns usually had a small contribution from the first order modes as well. These higher order modes never fully turn on as the current is increased. Instead the central peak tends to move over to one side. Externally measured directional shifts as large as 6° (implying a directional shift of 1.5° within the higher index cavity) have been observed. These shifts result from a change in the injected carrier, and hence gain distribution. In a properly fabricated CSP laser such shifts would not be able to occur even in aged lasers exhibiting larger degrees of gain flattening[45].

RELIABILITY

Five lasers from each of slices L78-54 and L78-55 which posessed sharp lasing turn-ons were selected for life testing at elevated temperatures. The lasers were mounted on an aluminum bar which could be heated and operated continuously in laboratory air. A feedback system was employed to continuously adjust the laser drive current to maintain a constant 3.3 mW output (single facet from chip). A preliminary 150 hour burn-in at room temperature was used to separate out poor lasers. Surviving lasers were then heated up to a heat sink temperature of 50°C or 70°C. The drive current required to maintain the pre-set power output was recorded and frequent D.C. L-I plots were made. The lasers were deemed to have failed when a drive current 300 mA was unable to maintain the pre-set 3.3 mW output.

Half the lasers (2 from L78-55 and 3 from L78-54) failed in under four hours. A typical example of this behavior (fig. 22) showed the increased threshold and decreased efficiency characteristic of dark-line defects. The isotropically emitted spontaneous emission was viewed through the (n-side) contact using an infrared microscope. In all of these cases, dark-line defects in a <100> direction were observed (fig. 23). Dark-line defects (DLD's) are dislocation networks which contain a high concentration of non-radiative recombination sites. The injected carriers recombine non-radiatively in these areas giving them a dark appearance. The carrier population in these regions is not inverted and will absorb strongly at the lasing wavelength, causing an increase in the threshold and a decrease in the quantum efficiency.

DLD's have been shown to originate at dislocations which are originally present in the device, and which grow predominantly by a climb mechanism into a 3-D network crossing the active layer in a mainly [100] direction[27]. Both optical excitation[28] and electron beam injection[29] have been shown to result in the growth of the DLD from a "seed" dislocation indicating the need of carrier recombination for DLD growth. A phonon-kick model[30], whereby all the energy released in a non-radiative recombination is given to a nearby atom, (reducing its activation energy for displacement) has been proposed as a mechanism for

the generation of the vacancy point defects by which the DLD climbs. The origin of the initial nucleation sites is uncertain. On the assumption that the dislocations in the substrate were initially distributed randomly and grew through the first confining layer into the active layer, only 2% of the lasers would be expected to fail from this cause. The fact that the longest lived laser L78-55/1 shared a mirror facet with L78-55/3 (early DLD failure) would seem to rule out strain-induced damage during some of the slice processing steps. Towards the end of this initial investigation it was discovered that the pre-epitaxy slice preparation was leaving contaminants on the GaAs surface. These contaminants could very easily act as DLD nucleation sites. A new cleaning procedure has since been instituted, and, as visibly smoother surfaces are now being grown, it is hoped that the reliability will be improved.

The other five lasers showed no signs of deterioration after 150 hours at room temperature and survived an additional 500 hours at a heat sink temperature of 50°C (active region temperature $\approx$63°C due to current heating) and an average of 90 hours at 70°C (active region temperatures $\approx$88°C). Using an activation energy of 0.7 eV which this lab has found to be appropriate under the given operation conditions[31], together with the active region temperatures, the average lifetimes extrapolated to room temperature were 1.5×10^4 hours with one laser (L78-55/1) lasting an equivalent of 3.2×10^4 hours.

The justification for using elevated temperatures as a means of extrapolating lifetimes back to room temperature is based on determining the degradation rate of the same laser at different temperatures. This experiment indicated that there was only one failure mechanism operating within the group of lasers tested. It was assumed that the failure mechanism had an associated activation energy, E_a, so that the lifetime t at a given temperature T could be written $t(T°K) \propto e^{E_a/kT}$. The value of 0.7 eV for E_a determined in this lab is in agreement with the value assigned by other experimenters[32]. This is somewhat surprising, considering that other workers have used different testing procedures and lifetime definitions.

As the lasers aged, the thresholds crept up (fig. 24) but the differential external quantum efficiency appeared to remain relatively constant. For laser L78-55/1 the external efficiency only started to visibly decrease in the final equivalent 6000 hr. of life. It was noticed that while the "kinks" generally seemed to originally occur at 4-5 mW optical power levels, they progressively became worse with time (fig. 25). It appears that the extra current drawn as the L-I curve becomes increasingly horizontal at a kink heats the active region, thus raising the threshold. As the L-I curve is now displaced further to the right (higher current) more current is forced through the device. This positive feedback appreciably speeds the decay rate as can be seen from the final few hours of L78-55/1 (fig. 24).

The response of the lasers to a square current pulse showed no spontaneous spiking after either 6600 hr (equivalent) or 'failure'. This phenomenon had been reported by Paoli[33] for similarly aged lasers and apparently indicated internal cavity changes which could not be observed externally. The null result is not conclusive as the expected frequency of oscillation (~1 GHz) could only barely be detected by the APD used (risetime = 0.6 ns).

The particular aging method used was chosen to simulate lifetimes of lasers in the field. The varying current, high optical flux at the surface, air ambient and extremes in temperature made it difficult to isolate the primary failure mechanism. One laser (L78-55/9) definitely failed as a result of a deterioration of the thermal bond, which may also have been a contributing effect in one other (L78-54/7). Ritchie et al[40] observed similar indium bond failures at higher temperatures and discovered that Au-In intermetallics had formed locally. That all the lasers in the present study did not show a thermal bond deterioration suggests that more attention be paid to this fabrication step as the present manual soldering allows for apparently significant chip to chip bond differences[41].

The failed lasers were inspected by an SEM at high magnification (x20,000) but damage to the mirror facets was not observed as had been

reported by several workers[42]. This is encouraging because although this failure mechanism can be prevented by Al_2O_3 facet coatings, there are practical problems associated with their deposition. As this mechanism is assumed to be photo-induced, it will likely have a strong optical power dependance. Lifetime comparisons with lasers operated at higher output powers would be useful to find the levels at which this failure mechanism becomes prominent.

Although the active region of the longest lived laser and the laser with a degraded thermal bond were relatively uniform after high temperature "failure", the remaining three had 2-4 large DLD's crossing the region in a <011> direction (ie. perpendicular to the cavity length). The apparent shift in DLD direction between the short and long-lived lasers may indicate a difference in the growth mechanism in the two cases but due to the small number of lasers studied this observation may only be coincidence.

The longest lived laser had no DLD crossing its active region, although it was not uniform in width along its length. The aging mechanism in this laser appeared to cause a spatially uniform decrease in the internal quantum efficiency. The cause of this degradation is not known, although Lang et al[43] demonstrated that for their lasers electron traps in the proton bombarded region had moved into the active layer during laser operation.

Aging data for oxide stripe CSP lasers was compared with proton-bombarded lasers fabricated from the same slice. The most striking feature of the oxide stripe aging behavior was the rapid degradation of the device after it had apparently settled down to a slow degradation rate. An extreme example of this can be seen in fig. 26 where the laser is seen to have died in less than three hours after having survived 330 hours at 50°C. This failure mode cannot be attributed to the simple downward passage of a kink because pulsed L-I data taken after failure shows no light output at all. Viewing of the active region required the injection of 100 mA (vs. about 5 mA for the photos in fig. 21) in order to see that almost the whole active region was dark. As the dark region was

not sharply defined, it was not possible to ascertain what fraction of the dislocation network was composed of <100> DLD's and what of <110> DLD's. The rapid growth rate in the <01$\bar{1}$> indicates that a <110> DLD is present running the length of the cavity and in addition having <100> DLD's nucleating off from it. As <110> DLD's are believed associated with external stresses[46] and this particular failure mode is rarely seen for proton bombarded devices, the cause of failure is tentatively attributed to stress caused by the proximity of the silicon dioxide mask to the active region.

Although the oxide stripe lasers did not last as long as the proton bombarded ones, their degradation rate until the sudden failure appeared to be marginally lower. The statistical sample was too small to make concrete conclusions on this point but it would be in agreement with the results of Lang[43] which demonstrated an increase in degradation rate with proton bombardment dosage.

DISCUSSION

The growth of one longitudinal mode at the expense of another indicates that the gain medium is homogeneously broadened as expected, given the short carrier-carrier scattering time ($\sim$ps)[34] as compared to the injected carrier lifetime. The rapid thermalization ensures that all the carriers respond identically to the incident radiation. Hence when the gain saturates at one frequency, it saturates over the whole spontaneous linewidth. This effectively pins the Fermi level separation and prevents other frequencies from ever reaching threshold.

The common experimental observation of multi-longitudinal mode operation from injection lasers has been attributed to spatial hole burning. The optical feedback supplied by the end mirror in a Fabry-Perot cavity selects out for amplification those frequencies whose round trip phase shifts are even multiples of 2π. Only a few passes through the gain medium are sufficient to transform the selected travelling wave spontaneous emission into the much more intense standing wave pattern characteristic of lasing in Fabry-Perot cavities. At the antinodes of the standing waves, the optical fields are sufficiently intense to locally saturate the gain. At the nodes, however, the carriers are not depleted and other longitudinal modes are able to pick up sufficient gain to lase.

Single longitudinal mode operation has, however, been observed, from TJS, CSP and, occasionally, narrow stripe lasers. It has also been achieved in the more complex distributed feedback laser[35] (DFB), which relies on a periodic perturbation of the active region for its mode selection. The existence of single longitudinal mode operation in the TJS laser was postulated by Streifer et al[36] as resulting from the very heavily doped p-type active layer used in that structure. Carriers diffuse from high carrier concentration regions (ie. optical nodes) to depleted areas (antinodes) as a rate dependent on the concentration gradient and the associated diffusion constant (ie. $\frac{\partial n}{\partial t} = -qD_n \cdot \frac{\partial n}{\partial x}$, in 1-Dimension). At the doping levels normally used in DH lasers ($1-5\times10^{17}$cm^{-3}), both the injected hole and electron concentrations

are greater than the background doping levels. In this limit, both species of charge carriers are constrained to diffuse together (amibolar diffusion) as a result of their mutual electrical attraction. Thus, the appropriate diffusion constant to be used is $D_{ambipolar} = 2\ D_{hole} = 2\ cm^2/sec$. The analysis by Danielmeyer[37] indicates that this low mobility will leave sufficient gain at the nodes for multimode operation. The heavy doping used in the TJS active layer ($N_A \approx 10^{19} cm^{-3}$) results in predominantly minority carrier (electron) injection which, as a result of the much higher background doping, can diffuse at their normal rate ($D_{electron} = 50 cm^2/sec$) without having to "drag" holes along with them. The higher diffusion rate reduces the gain at the nodes and permits only one mode to lase. Scifres et al[38] achieved single longitudinal mode operation with a broad contact (500 μm x 350 μm) conventional DH laser with heavy ($5x10^{18} cm^{-3}$) p-doping of the active layer in support of Streifer's model.

The observed single mode operation of CSP lasers cannot be explained by this theory because the active layer doping is the same as a conventional DH laser. The apparent success of the Streifer model when applied to TJS lasers suggests, however, that carrier diffusion may indeed be manipulated to reduce the occurence of multi-longitudinal modes. The primary difference between CSP and conventional lasers is their degree of transverse mode control. Lasers which rely on the carrier distribution for their mode control tend to oscillate in higher order transverse modes with differing longitudinal mode number. If the laser is constrained to oscillate in its lowest order transverse mode, gain "robbing" by higher order transverse modes is not possible and gain-competition is restricted to different axial longitudinal modes. At sufficiently high current levels the carrier depletion caused by the optical fields will be more pronounced, resulting in steeper axial concentration gradients than if higher order transverse modes were oscillating. The resulting increase in diffusive flow may be sufficient to keep other longitudinal modes from picking up sufficient gain in the node regions of the dominant mode. The increase in diffusive flow required for single mode operation may be only slightly above that for ordinary lasers. The reduction in gain for the

dominant mode, once another longitudinal mode starts to oscillate will be severe. This is due to the reduction of its sustaining diffusive currents. Support for the required small increase in diffusive flow, may come from more realistic values of the diffusion coefficients than those chosen by Streifer[36]. The ambipolar diffusion coefficient $D_{amb} = \frac{D_n D_p (N_p + P_p)}{D_n N_n + D_p P_n}$. Using data taken from Sze[39] for mobilities at the doping concetrations $N_a = 5 \times 10^{17}$ and $1 \times 10^{19} \mathrm{cm}^{-3}$ and the generalized Einstein relations (see fig. 9) the ratio of the diffusion coefficients in the two cases is only 1.5 as opposed to 25 claimed by Streifer.

It is clear that substantial diffusive flow must take place in order to avoid saturation of the L-I characteristic at the very high power levels observed by Aiki et al[15]. If the carrier diffusion is strong enough to withstand slight variations in the position of the gain peak then a skipping over of certain longitudinal modes may be expected as a result of changes in excitation or temperature.

CONCLUSIONS

A preliminary attempt at fabricating channeled-substrate planar lasers has been made with encouraging results. Despite the lack of significant improvement in device linearity (resulting from a thick first confining layer) low thresholds, high efficiencies and long lifetimes have been demonstrated. Single longitudinal mode operation implies at least a small improvement in mode control.

The second generation of CSP lasers has thinner first confining layers which should result in better mode control. Improved pre-growth slice preparation has resulted in smoother as-grown surfaces which makes slice processing easier and in particular will reduce the spread in threshold values. A side benefit of the cleaner substrate is anticipated to be a much greater device yield due to a reduction of DLD nucleation sites.

References

1. Burrus, C.A. and Dawson, R.W. Applied Physics Letters 17 (1970). p. 97

2. Keck, D. Fundamentals of Opticl Fiber Communication, Barnowski, M. (ed). Academ Press, New York, 1976.

3. Marton, J.P. Optical Communication lecture notes. McMaster Engineering Physics 4K3 (1976).

4. Casey, H.C. and Panish, M.B. Heterostructure Lasers Part B. Academic Press, New York 1978 p. 207.

5. Paoli, T.L. IEEE Journal of Quantum Electronics QE-12 (1976) p. 770.

6. esp. for coupling into single mode fibers. see Dixon, R.W., Nash, F.R., Hartman, R.L., Hepplewhite, R.T. Applied Physics Letters 29 (1976) p. 372.

7. Arnold, G. and Petermann, K. Optical and Quantum Electronics 10 (1978) p. 311.

8. Chinone, N. Journal of Applied Physics 48 (1977) p.3237

9. Dyment, J.C. Applied Physics Letters 10 (1967) p. 84.

10. Ibid 4.

11. Campos, M.D., Hwang, C.J., Bossi, R.I. and Ripper, J.E. IEEE Journal of Quantum Electronics QE-13 (1977) p. 687

12. Ibid 5.

13. Oomura, E., Hirano, R., Tamaka, T., Ishii, M., and Susaki, W. IEEE Journal of Quantum Electronics QE-14 (1978) p. 460.

14. Frescura, B.L., Hwang, C.J., Leuchinger, H. and Ripper, J.E. Applied Physics Letters 31 (1977) p. 770.

15. Tsukada, T. Journal of Applied Physics 45 (1974) p. 4899.

16. Aiki, K., Nakamura, M., Kuroda, T. and Umeda, J. Applied Physics Letters 30 (1977) p.649.

17. Kirkby, P.A. and Thompson, G.H.B. Journal of Applied Physics 47 (1976) p. 4578.

18. The lasing wavelength is always longer than the wavelength of the spontaneous emission peak but since a small amount of Al has been added to the active layer, the lasing frequency is very near the peak of the absorption spectrum of the pure GaAs substrate.

19. Aiki, K., Nakamura, M., Kuroda, T., Umeda, J., Ito, R., Chinone, N. and Maeda, M. IEEE Journal of Quantum Electronics QE-14(1978) p. 89.

20. Nash, F.R. Journal of Applied Physics 44 (1973) p. 4696.

21. Ibid 4, p. 176.

22. Kressel, H. and Butler J.K. Semiconductor Lasers and Heterojunction LED's. Academic Press New york 1977 p. 275.

23. Bernard, M. and Duraffourg, G. phys. Stat. Solidi 1 (1961) p. 699.

24. Ibid 4.

25. Nakamura, M., Aiki, K., Chinone, N., Ito, R., Umeda, J. Journal of Applied Physics 9 (1978) p. 4644.

26. Joyce, W.B. and Dixon, R.W. Journal of Applied Physics 46 (9175) p. 855

27. DeLoach, B.C., Hakki, B.W., Hartman, R.L., D'Asaro, L.A. Proceedings of the IEEE 61 (1973) p. 1042.

28. Woolhouse, G.R., Monemar, B. and Serrano, C.M. Applied Physics Letters 33 (1978) p. 94.

29. Petroff, P.M., and Kimmerling, L.C. Applied Physics Letters 29 (1976) p. 461.

30. Ibid 22. p. 547.

31. private communication with J.C. Dyment.

32. Hartman, R.L. and Dixon, R.W. Applied Physics Letters 26 (1975) p. 239.

33. Paoli, T.L. Techn. Digest 1976 Int. Electron Devices meeting (1976) p. 136.

34. Nishimura, Y. Jpn. J. Appl. Phys. 13 (1974) p. 109.

35. Aiki, K., Nakamura, M., Umeda, J. IEEE Journal of Quantum Electronics 12 (1976) p. 597.

36. Streifer, W., Burnham, R.D., Scifres, D.R., IEEE journal of Quantum Electronics 13 (1977) p. 403.

37. Danielmeyer, H.G. Journal of Applies Physics 42 (1971) p. 3125.

38. Scifres, D.R., Burnham, R.D. and Streifer W. Applied Physics Letters 31 (1977) p. 112.

39. Sze, S.M. Physics of Semiconductor Devices Wiley Interscience Toronto 1969 p. 49,99.

40. Ritchie, S., Godfrey, R.F., Wakefield, B. and Newman, D.H. Journal of Applied Physics 49 (1978) p. 3127.

41. as the bonds were made by an inexperienced worker (the author), this effect may be negligible in standard processesed lasers.

42. Chinone, N., Nakashima, H., and Ito, R. Journal of Applied Physics $\underline{48}$ (1977) p. 1160.

43. Lang, D.V., Hartman, R.L., Schumaker, N.E. Journal of Applied Physics $\underline{47}$ (1976) p. 4986.

44. Ibid 22.

45. N. Chinone, private communication.

46. Yamakoshi, private communication.

FIG. 1 Emission Characteristics for both mirrors of same DH Ga$_{1-x}$Al$_x$As Laser.
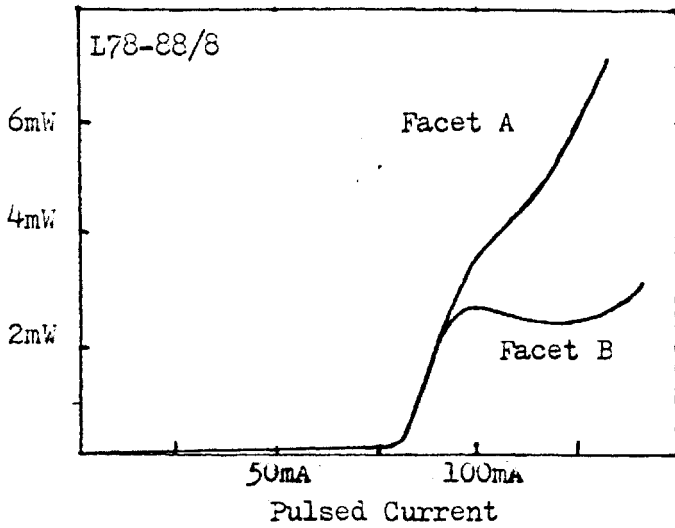
FIG. 2 Pictoral Representation of Lateral Current Spreading from Top Metalized Contact.

L78-88/8

6mW

Facet A

4mW

2mW

Facet B

50mA   100mA

Pulsed Current

metal electrode
p$^+$ capping layer

2nd
confining
layer
active layer

1st confining layer

X

Y
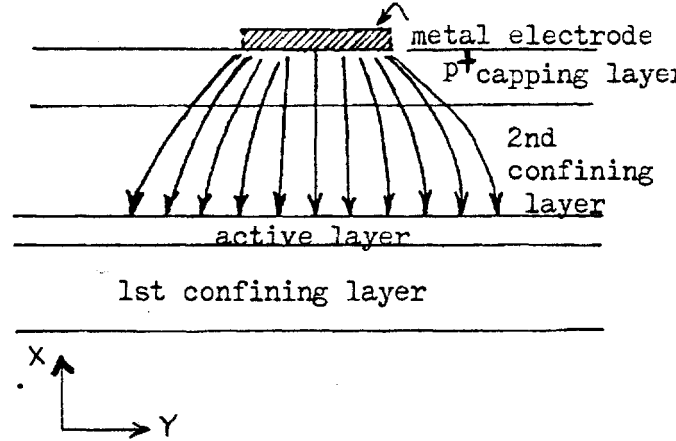
FIG. 3 Comparison Between Near Field Optical Distribution and Resultant Far Field Pattern as a Function of Stripe Width.

S=10μm   m=0

20μm   m=1

20μm   m=2

30μm   m=3

30μm   m=4

50μm

10μm

0 I RADIAN

m=12

(a)   (b)

NOTE that as transverse mode number (m) increases, maxima in near field moves away from stripe center.
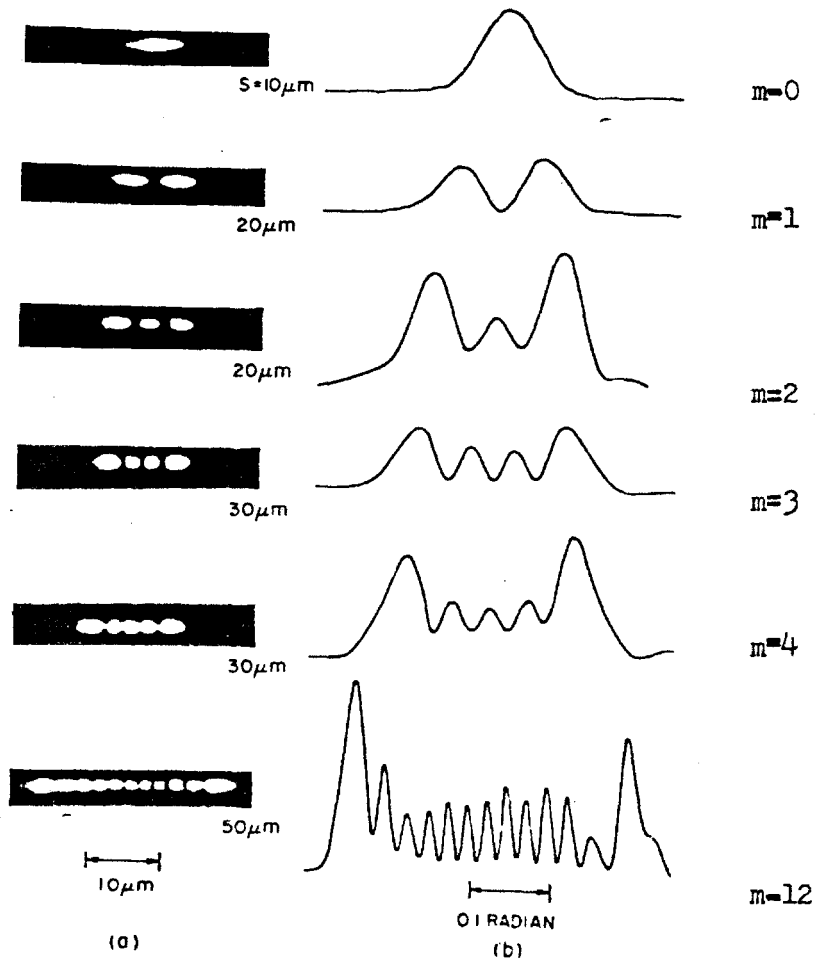
FIG. 7.11-2   Modes along the junction plane as a function of stripe width S for planar-
stripe DH lasers. (a) Near field patterns. (b) Far field patterns.

FIG. 4 Theoretical Calculation
Demonstrating Gain Saturation
for 8μm wide contact stripe.

Distance across Active Region
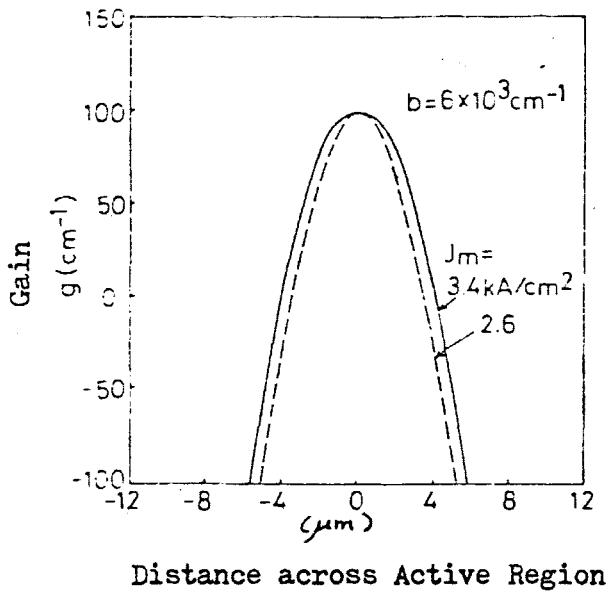
FIG. 5 Groove in Substrate and its
Effect on the Final Device.

a) End View of CSP Laser
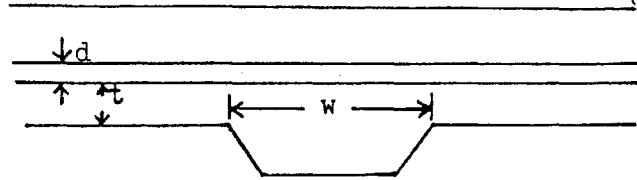
b) Approximate Representation of
Above Situation.
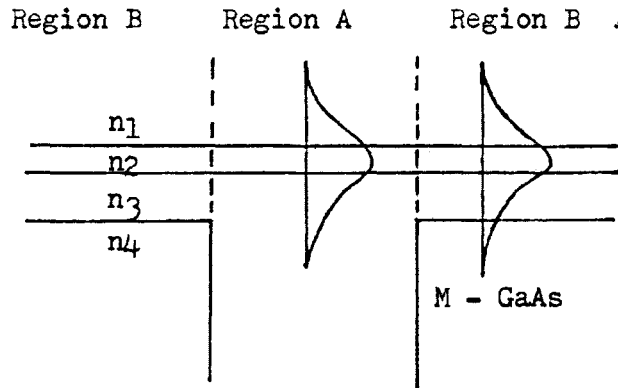
FIG. 6   Theoretical Calculations Relating Active Layer Thickness (d)
and first confining layer thickness (t) to the effective
index change $\Delta \tilde{n} = \Delta n + i \Delta \alpha / 2 k_0$
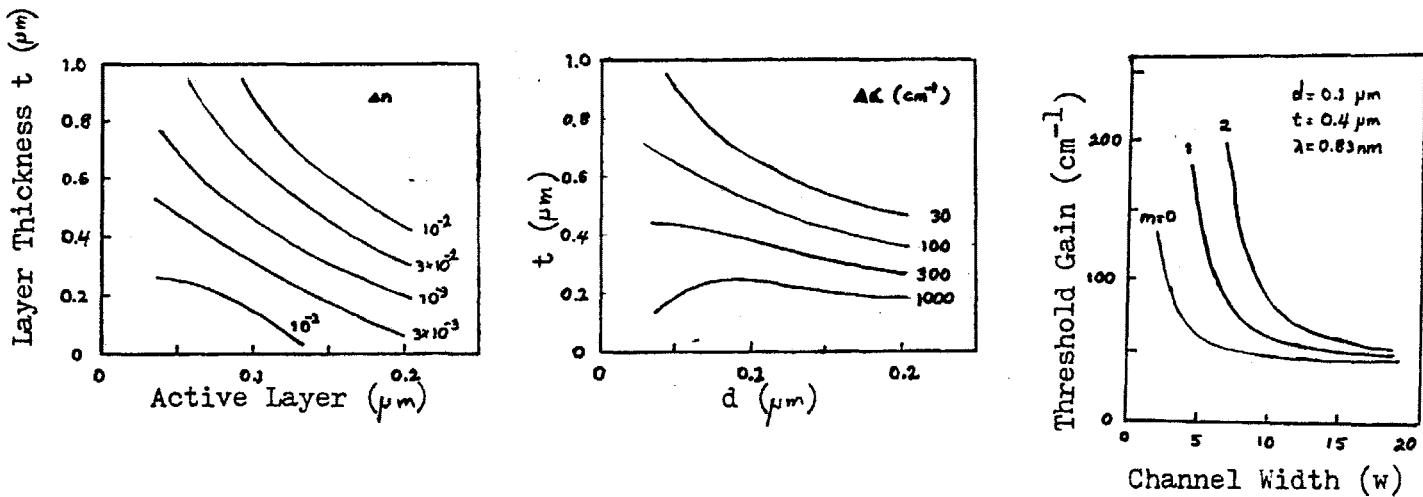
FIG. 7 $[01\bar{1}]$ on (100) Face Determined by Preferential Etch through Oxide Mask.

x//O
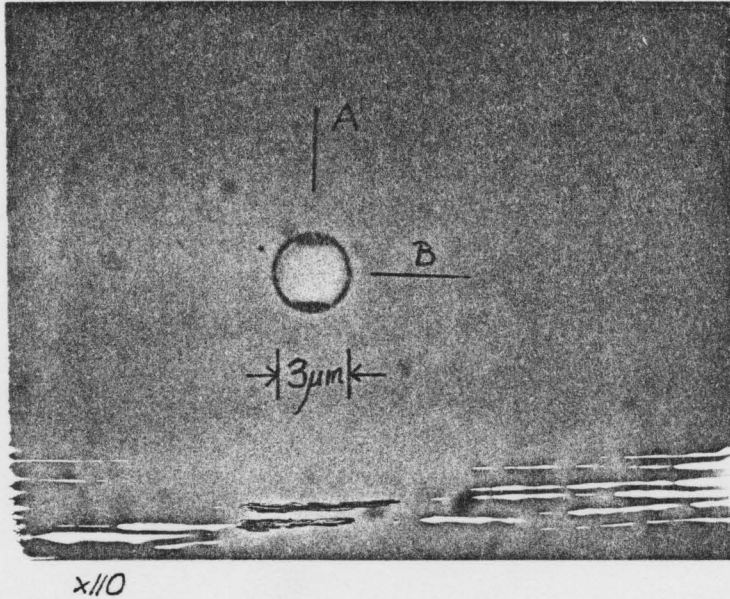
Cross section if cleaved along line A.
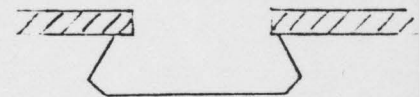
Cross section if cleaved along line B.

FIG. 8 Directional Dependance of Slow Etch Planes When a Specific Preferential Etch is Used on a Zinc Blend Structure.
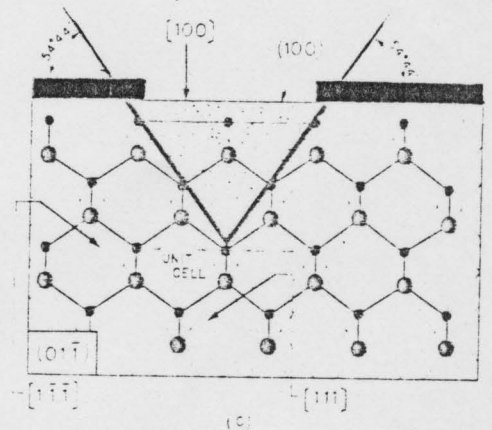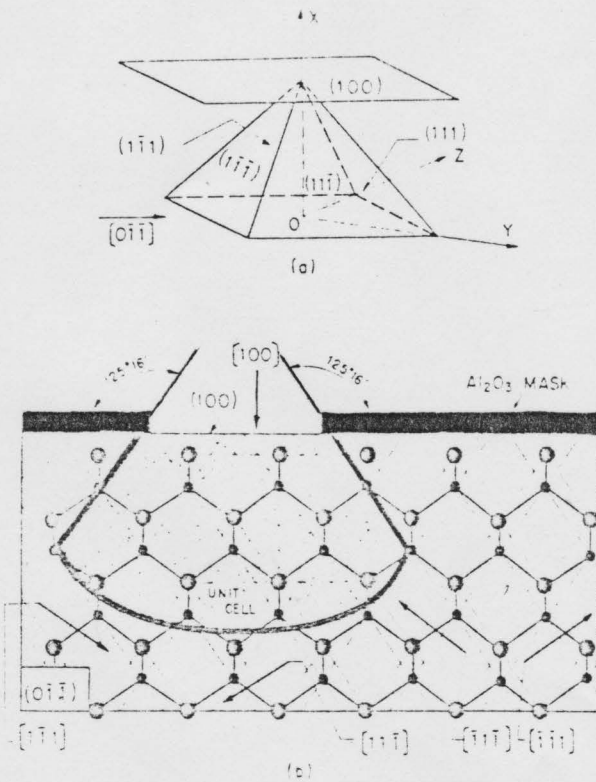
Fig. 8. Schematic diagrams of cross sections etched in {100} planes for zinc blende structure by perspective drawing through {110} planes and of relation between {100} and A{111} or B{111} planes: ● = group III; ● = group V atoms; (a) = relation between {100} and A{111} or B{111}; (b) = cross section of a channel etched parallel to $[01\bar{1}]$ in {100}; (c) = cross section of a channel etched parallel to $[0\bar{1}\bar{1}]$.

Figure 9: Theoretical Calculations for as grown structure.
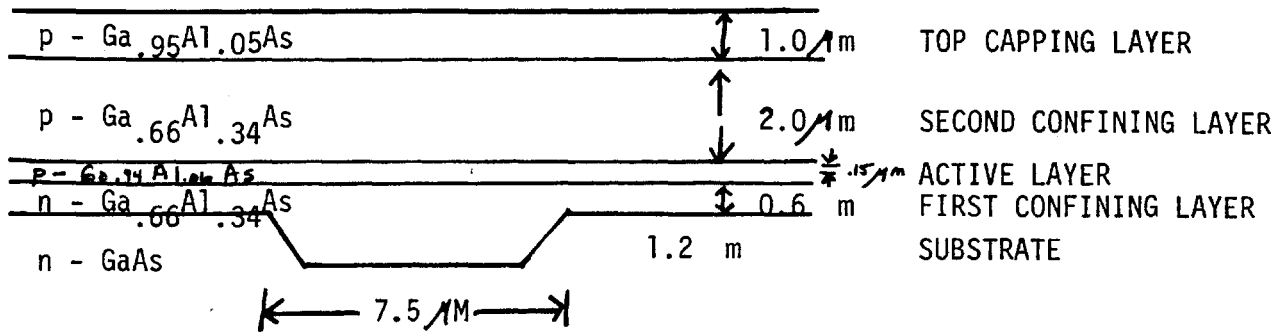
$\Delta x \equiv$ Difference in fractional aluminum concentration between confining and active regions = 0.34 - 0.06 = 0.28

$\Delta n \equiv$ Dielectric step between active and confining layers
$\simeq 0.62 \Delta x$ (for $\lambda \sim 9000\text{Å}$) = 0.17

$E_{GAP} = 1.424 + 1.266x + 0.266x^2$ (eV) for $Ga_{1-x}Al_xAs$ where $x < 0.37$

$E_{GAP}(x=0.30) = 1.89eV$; $E_{GAP}(x=0.06) = 1.50eV$ $\therefore E_{GAP} = 0.39eV$

$\Gamma_m \simeq$ Radiation Confinement Factor for m^{th} mode = 0.5 (m=0)

Beam Width $\perp$ to Active Layer = 47° (Full Width at Half Maximum)

Maximum Electric Field at Facet for 5mW operation = 14.9kV/cm.

$\alpha_{fc} \equiv$ Free Carrier Absorption in Active Layer at Threshold
$(N_a = 5 \times 10^{17} \text{ cm}^{-3}) = 24 \text{ cm}^{-1}$

$\alpha_{fc,x} \equiv$ Free Carrier Absorption in Confining Layers $(N_o \sim N_a \sim 3\times10^{17}) = 3\text{cm}^{-1}$

$\alpha_{SCATT} \equiv$ Scattering Losses from Cavity Imperfections $\sim 5 \text{ cm}^{-1}$

$\alpha_{COUPLING}$ = Losses Resulting from Umpumped GaAs within Evanescant Tails
$\sim 0 \text{ cm}^{-1}$

$m \equiv$ Mode Number

$\mathcal{L} \equiv$ Cavity Length = $250 \mu m$

$R_m \equiv$ Modal Facet Reflectivity $\simeq 0.34$ For TE Polarization and m = 0
with $\Delta n/n_{active}$ = 4% and $d = 0.15 \mu m$

$\Gamma_m g_{th}$ = Gain per unit length required to equal cavity losses.
$= \Gamma_m \alpha_{fc} + (1-r_m) \alpha_{fc,x} + \alpha_{SCATT,m} + \alpha_{COUPLING,m} - 1/L \ln(R_m) = 60.5 \text{ cm}^{-1}$
$g_{th} = 121\text{cm}^{-1}$

. . . 2

Figure 9: Theoretical Calculations for as grown structure (con't)

J_{th} = Threshold Current Density (ie. Current density at which Gain=g_{th})

$\quad$ = $(d/\eta_i)\left\{(g_{th}/\beta_s) + J_1\right\}$ $\quad$ Where β_s =0.044 cm/A, J_1=5300 A/cm^2 at

$\quad$ T = 300°K

$\quad$ = 1725 A/cm^2 $\quad$ Assuming η_i=0.7

η_{ext} $\equiv$ External Differential Quantum Efficiency

$\quad$ = η_i (ln 1/R$_m$)/(L Γ_m g_{th}) =0.53

$\Delta\lambda\equiv$ Wavelength Separation between Adjacent Longitudinal Modes

$\quad$ = $\lambda_L^2 \left\{2\pi L\left[1-\left(\lambda_L/\pi\right)^{2\pi}/2\lambda\right]\right\}^{-1}$, $\quad \frac{\partial n}{\partial \lambda} \approx 0$ @ $\lambda \approx 0.84\mu m$

$\quad$ = 3.9 $\overset{\circ}{A}$ at λ_L =8450 $\overset{\circ}{A}$

FIG. 10 Device Lifetime as a Function
of Emission Wavelengths for
LED's Operated at 1000 A/cm^2.
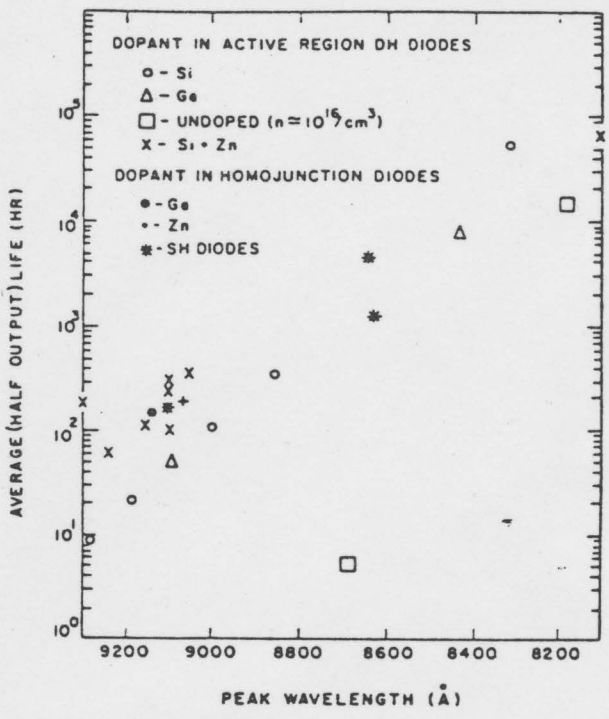
FIG. 11 Final Bonded Device
Configuration.
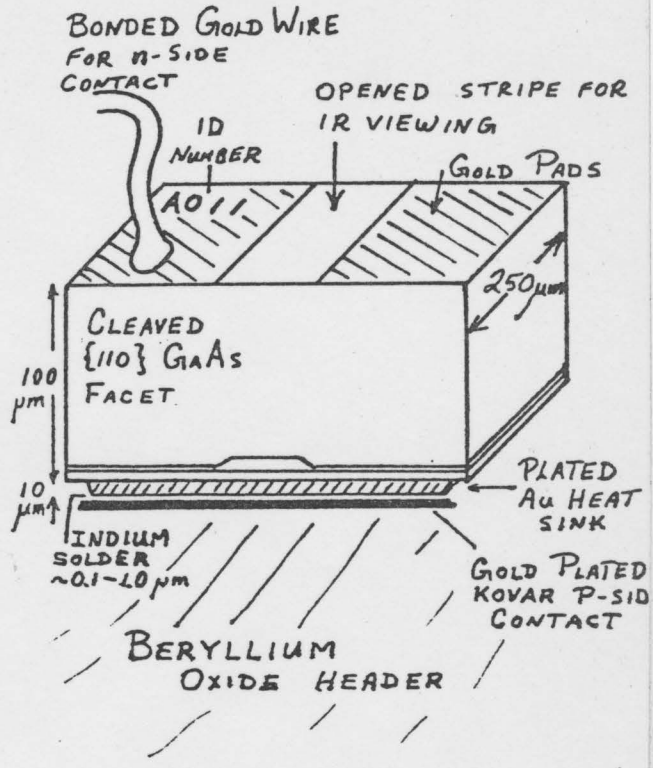
FIG. 12 SEM Photo of Cleaved Mirror (x5000 mag.)
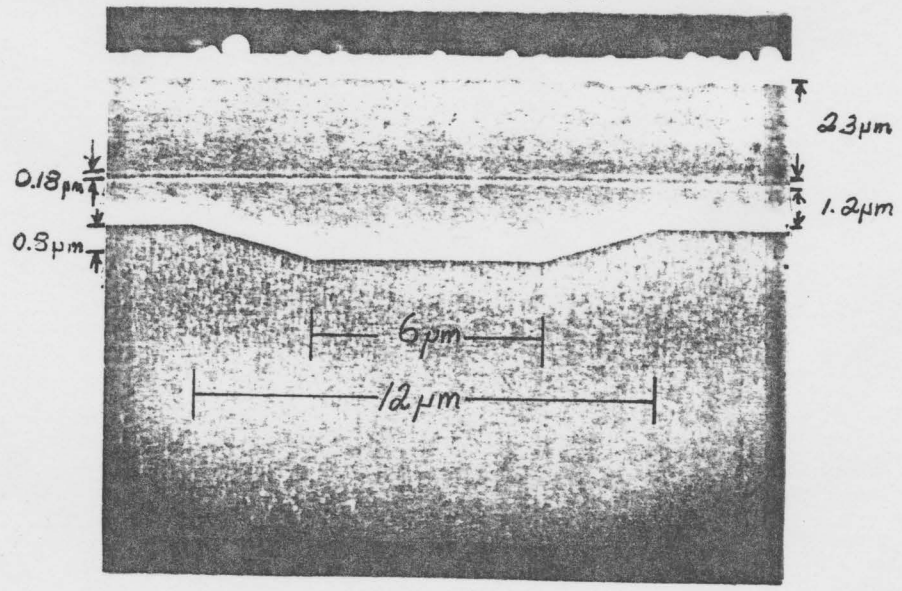
FIG.13. Top view of as-grown slice (x110 Mag.) showing terraced regions over channel.
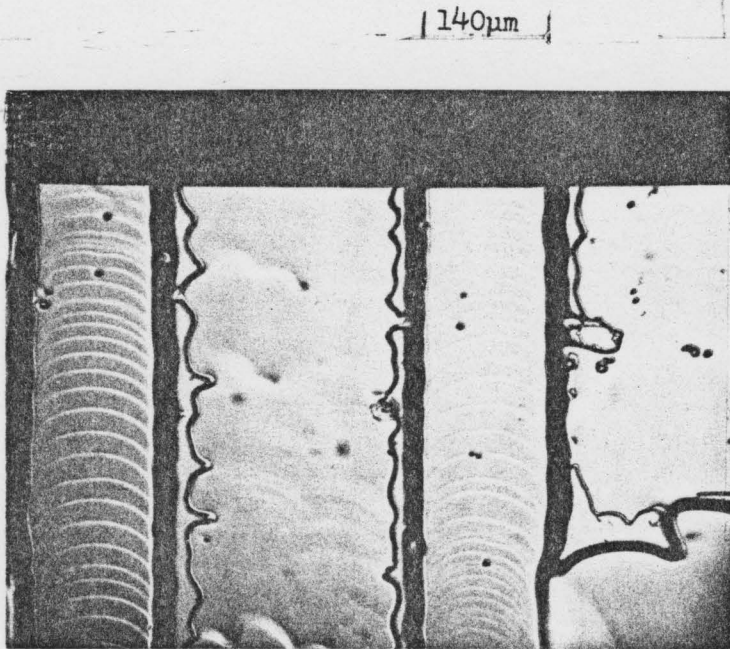
after channel locating etch

|140μm|
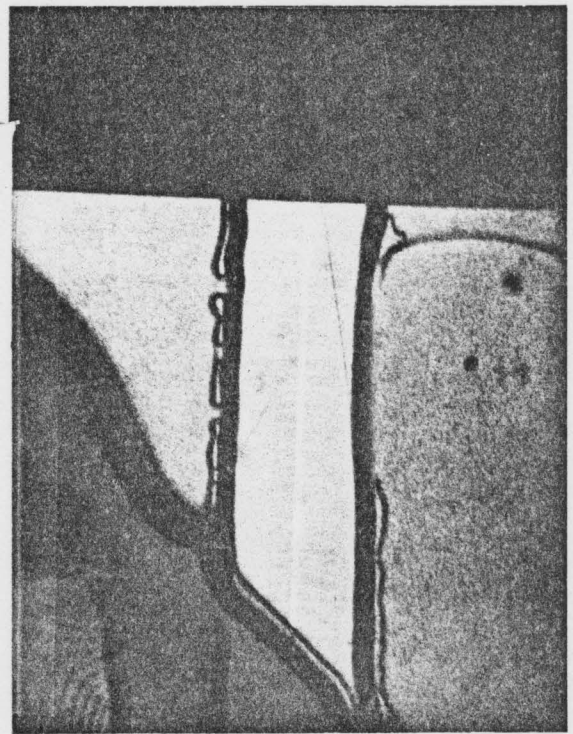
FIG.14 Average Pulsed Current Thresholds.

Slice No.	Oxide Stripe	Proton Bombarded
L78-52	140mA (100mA)*	140mA (120mA)*
L78-54	120mA (105mA)*	115mA (65mA)*
L78-55	200mA (160mA)*	100mA (70mA)*

* current values given in parentheses are the lowest thresholds observed within each group.

FIG.15 Varation of J_{th} as a function of stripe width for DH lasers at Room Temperature.
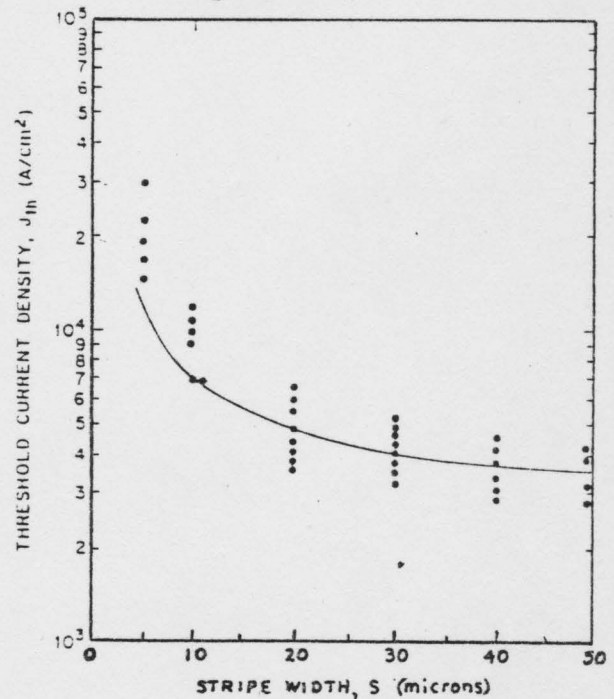
FIG. 16 Representative pulsed L-I characteristics of Proton-Bombarded lasers from two different slices.
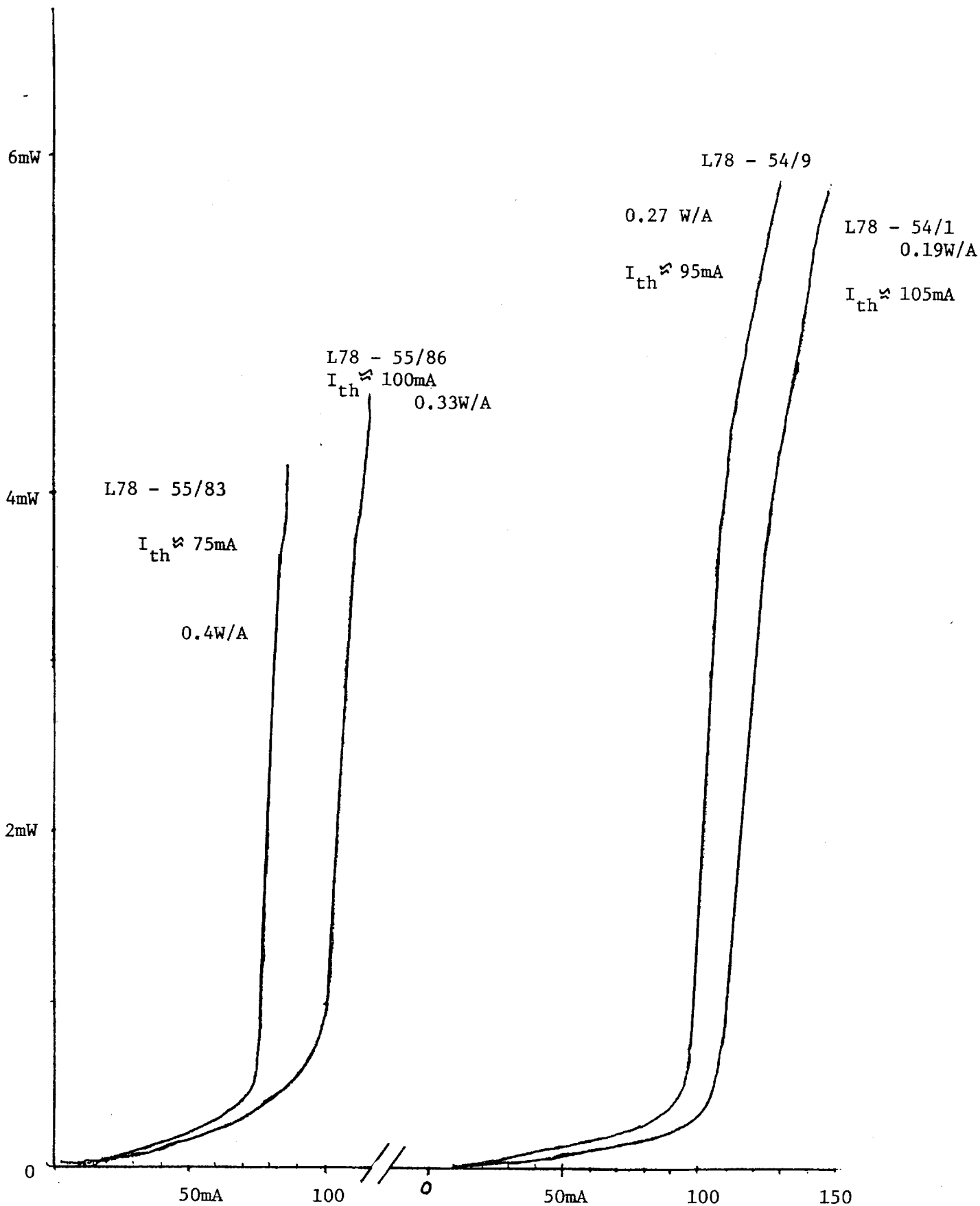
FIG. 17 Pulsed and D.C. L-L plots illustrating the thermal resistance of lasers bonded onto XO-72 headers using plated Indium as the bonding agent.

Text within figure:

I_{th} (PULSE) = 75 mA

I_{th} (D.C.) = 77 mA

⟨R⟩ = 27 °C/w

η_{ext} = 0.36 W/A

TOP VIEW OF XO-72 PACKAGE

KOVAR LEADS

BeO₂

LASER

SIDE VIEW
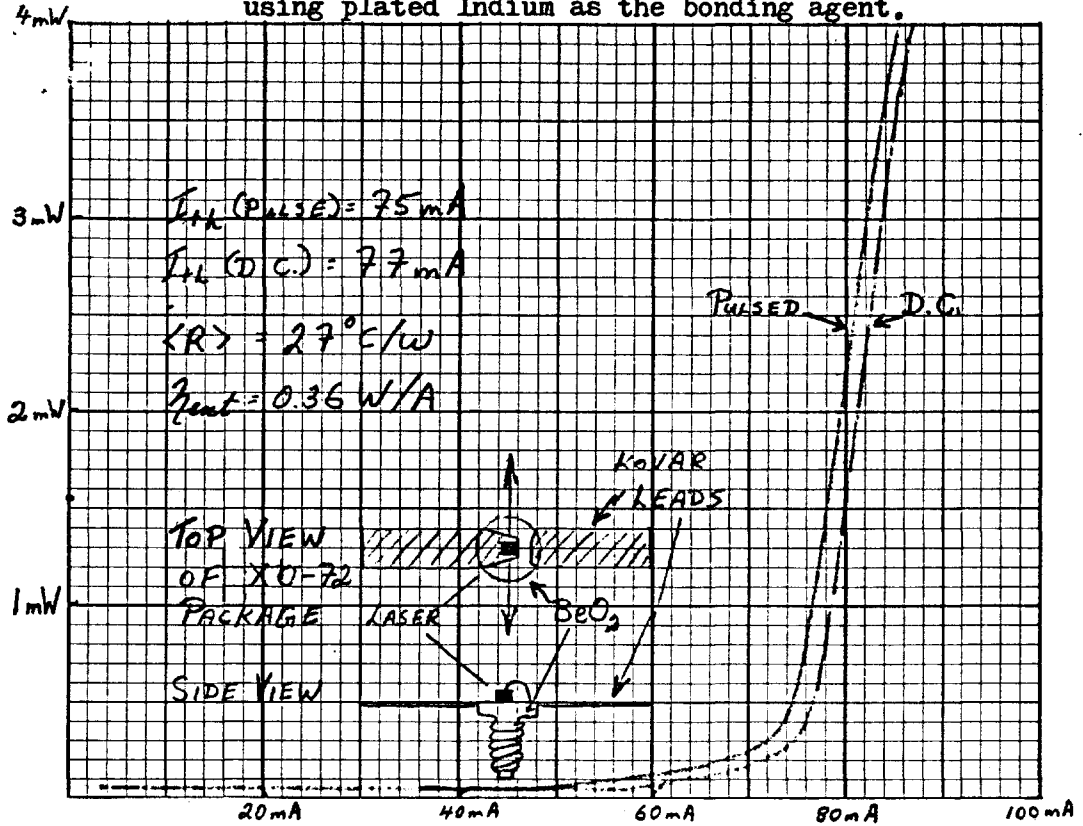
PULSED   D.C.

FIG. 18 Pulsed Threshold vs. heat sink temperature.

$I_{th}(T\,°k) = 9.2\,e^{T/38}$

for $T \leq 350°K$

ln (I_{th})

T (°K)
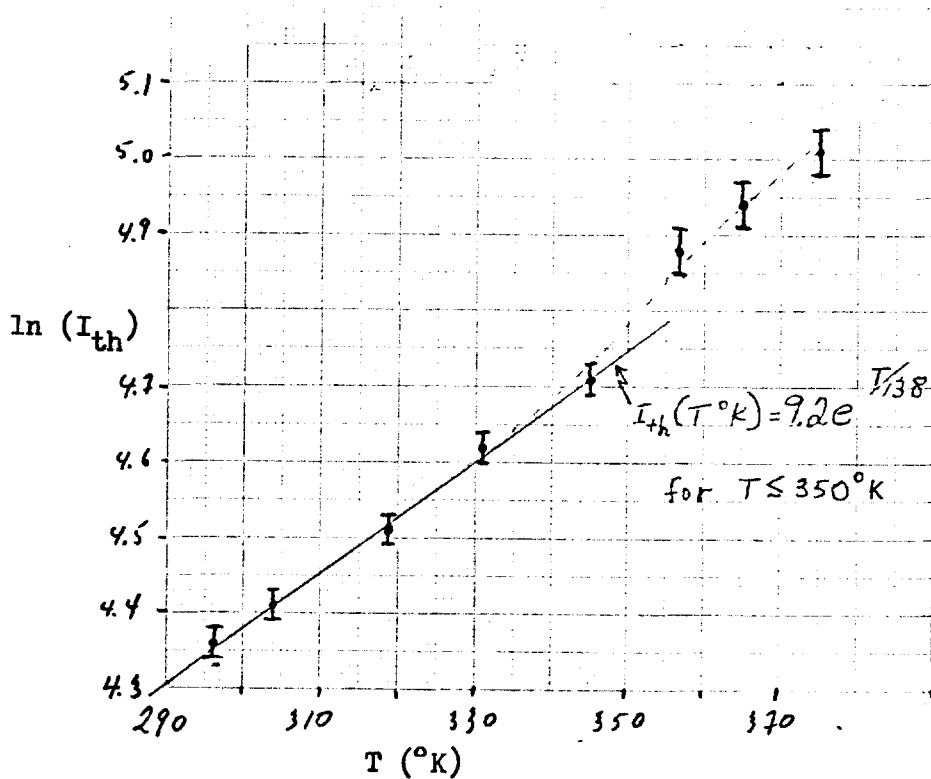
FIG. 19a. D.C. spectra below and just above threshold.

92.5 mA

90.0 mA

87.5 mA

8300   8400   8500   8600
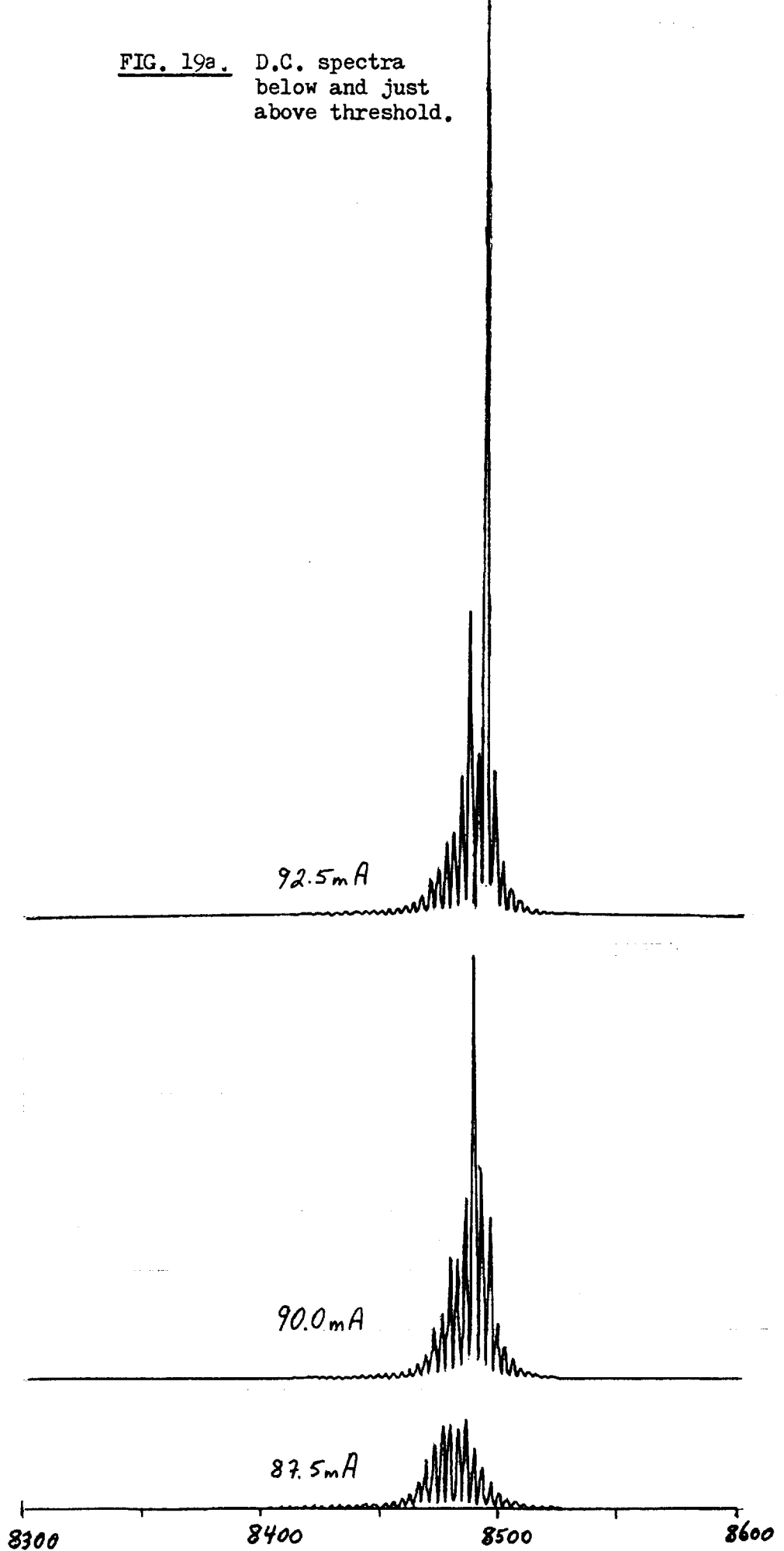
FIG. 19b. Spectra of laser operated with 1 µsec current pulses (1kHz rep rate).

FIG. 19(b)

$L\,78\text{-}55/77$
CHANNELED SUBSTRATE
LASER. $(I_{th} = 70\,mA)$

$I = 80\,mA$
$50\,\mu m$ slits

INSTRUMENT RESOLUTION $= 0.5\,\overset{o}{A}$

$\leftarrow 1.7\,\overset{o}{A}$

$1\,\overset{o}{A}$

LIGHT INTENSITY (ARBITRARY SCALE)

8240   8250   8260   8270   8280   8290   8300
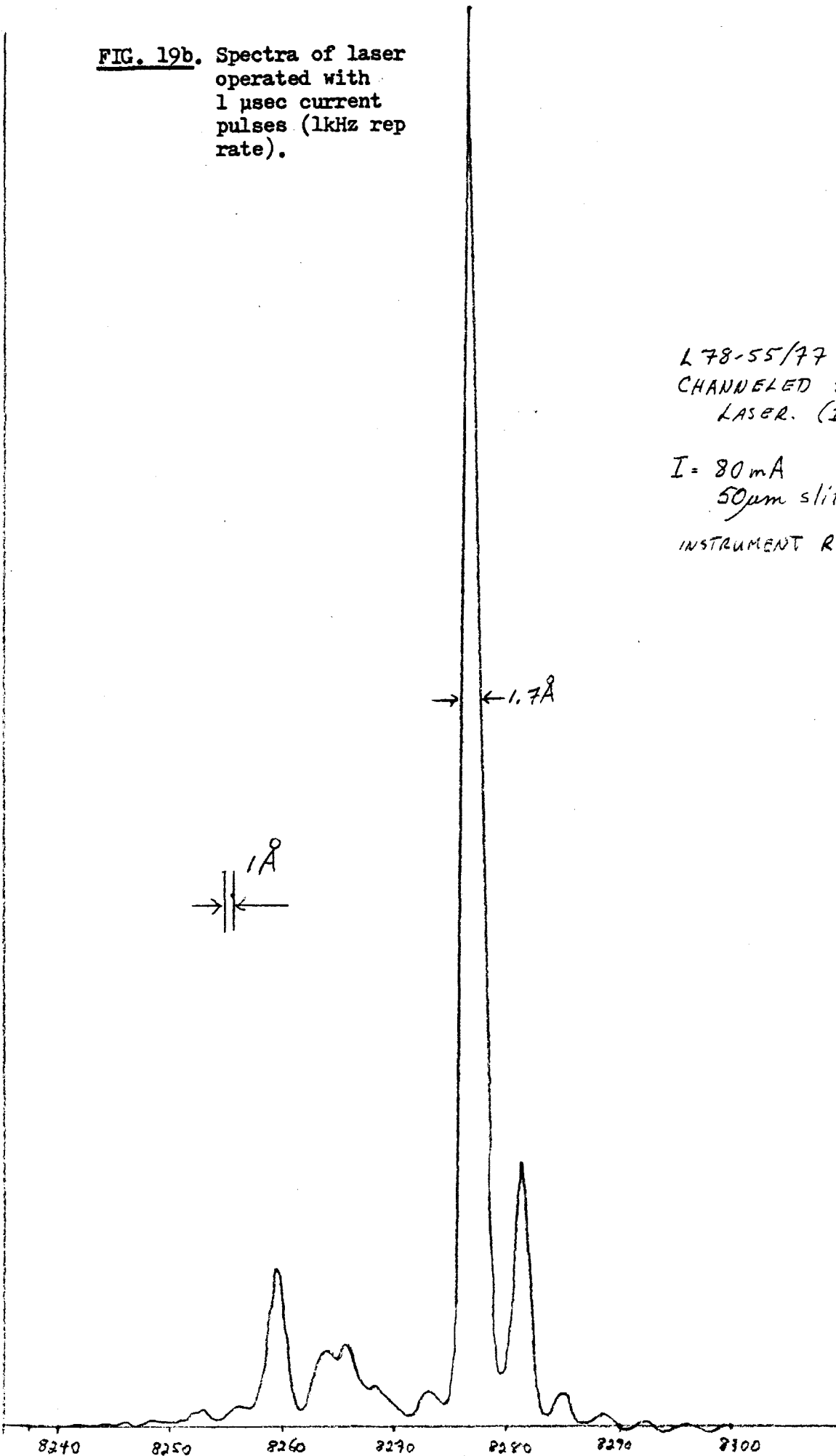
FIG. 20 High resolution spectra of CSP laser as pulsed current is varied.
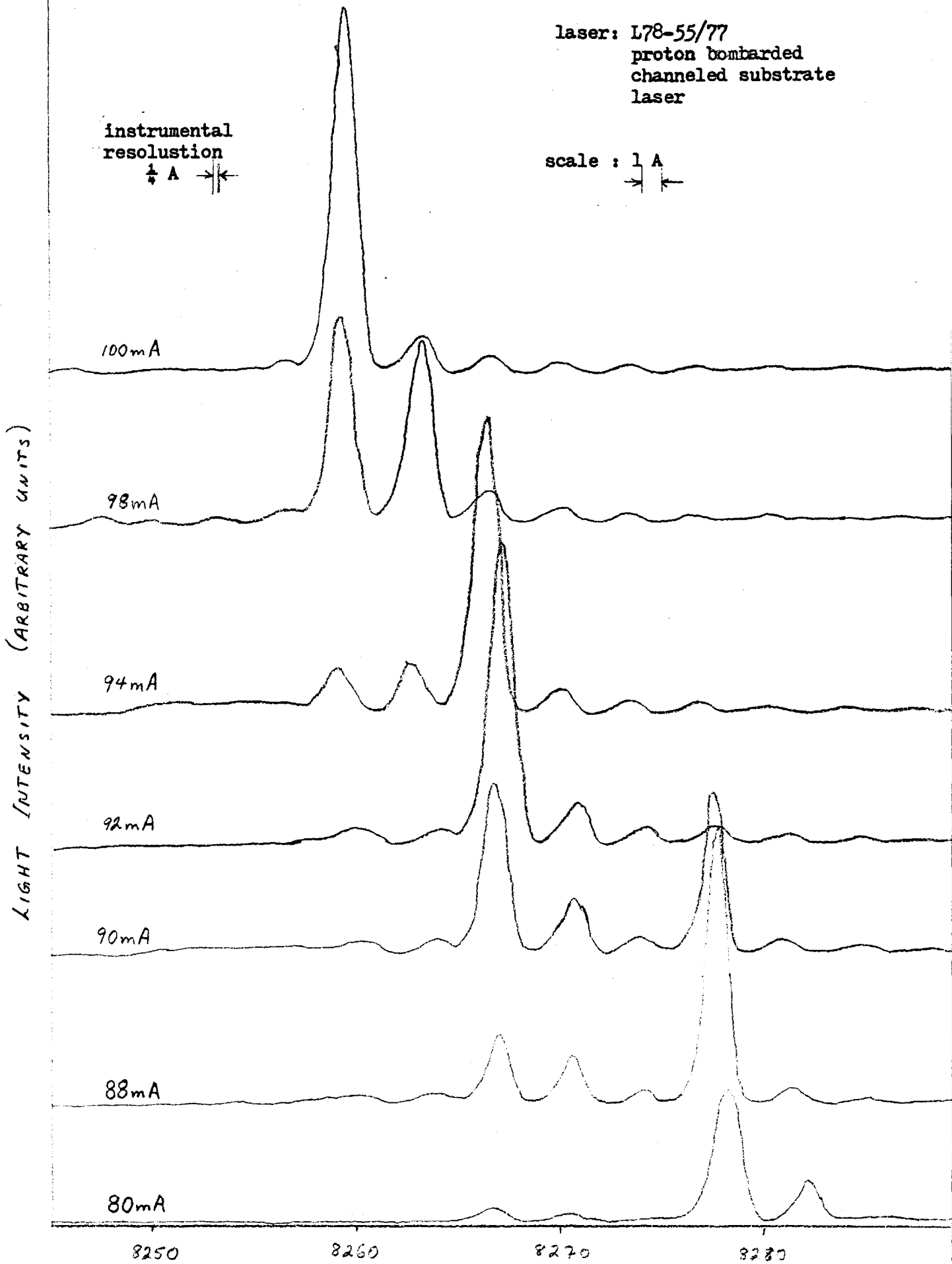
Figure 21 : Far Field Intensity Patterns as Recorded by CCD Array for L78-55/119

21. a. PARALLEL TO JUNCTION   I = 81mA
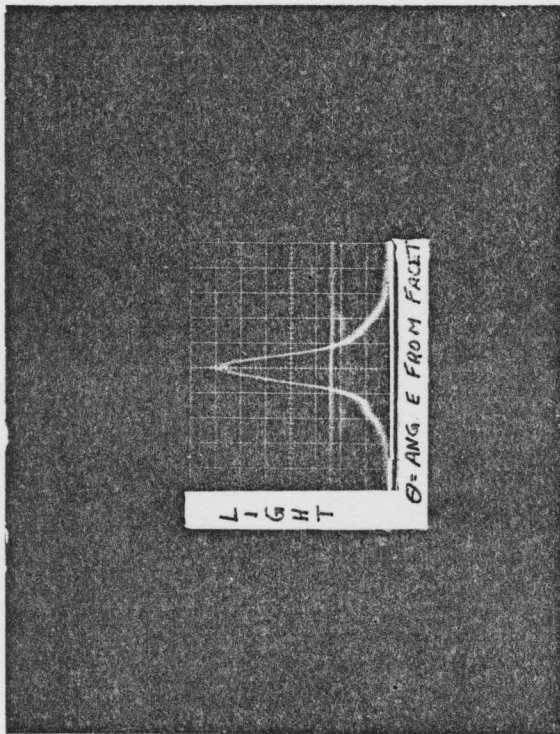
LIGHT INTENSITY (ARBITRARY SCALE)

Θ (1 SQUARE = 10.6° for all photos)

21. b.   I = 90mA
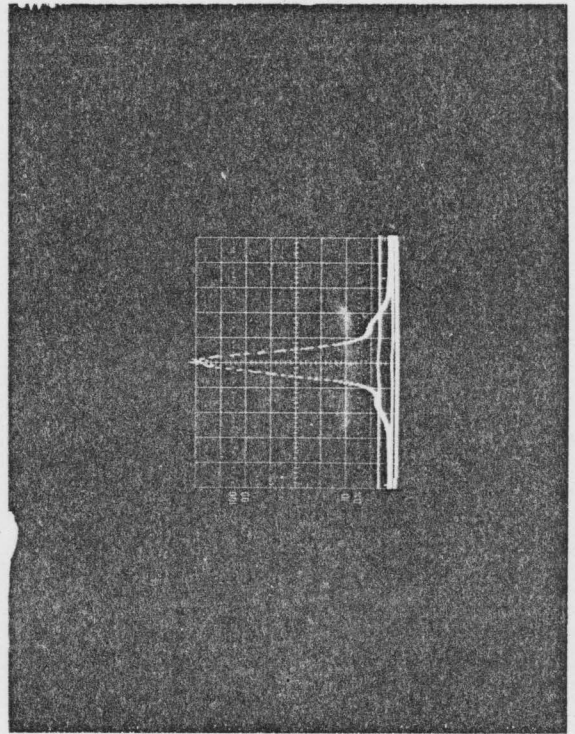
Note: The onset of the m=1 mode as the current is increased from 81 mA in 21.a. to 90 mA in 21.b.

21. c.   I = 128 mA
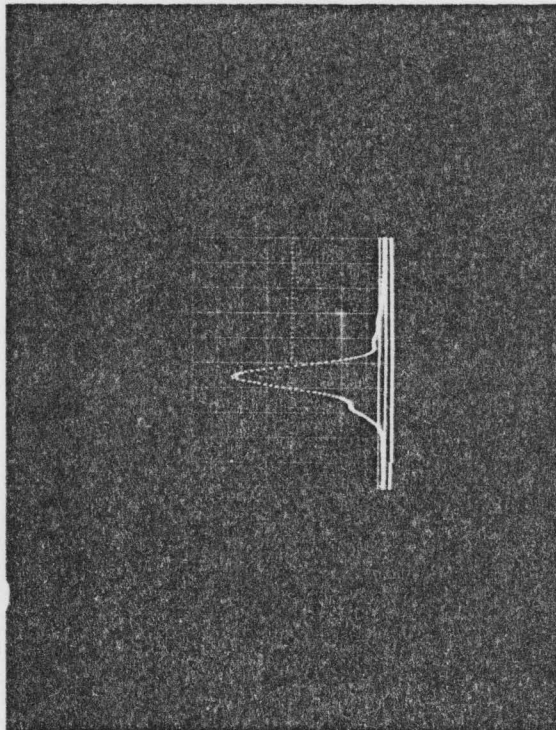
EXPERIMENTAL GEOMETRY SAME AS a.fb. NOTE SHIFT TO LEFT

21. d.   I = 128 mA
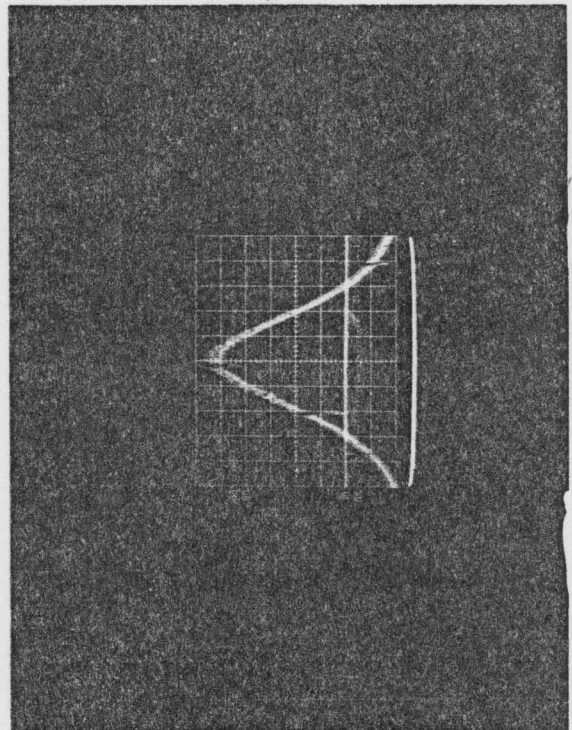
Fig.22 Typical light output vs. current behavior of a rapidly degrading laser recorded 12 minutes apart.
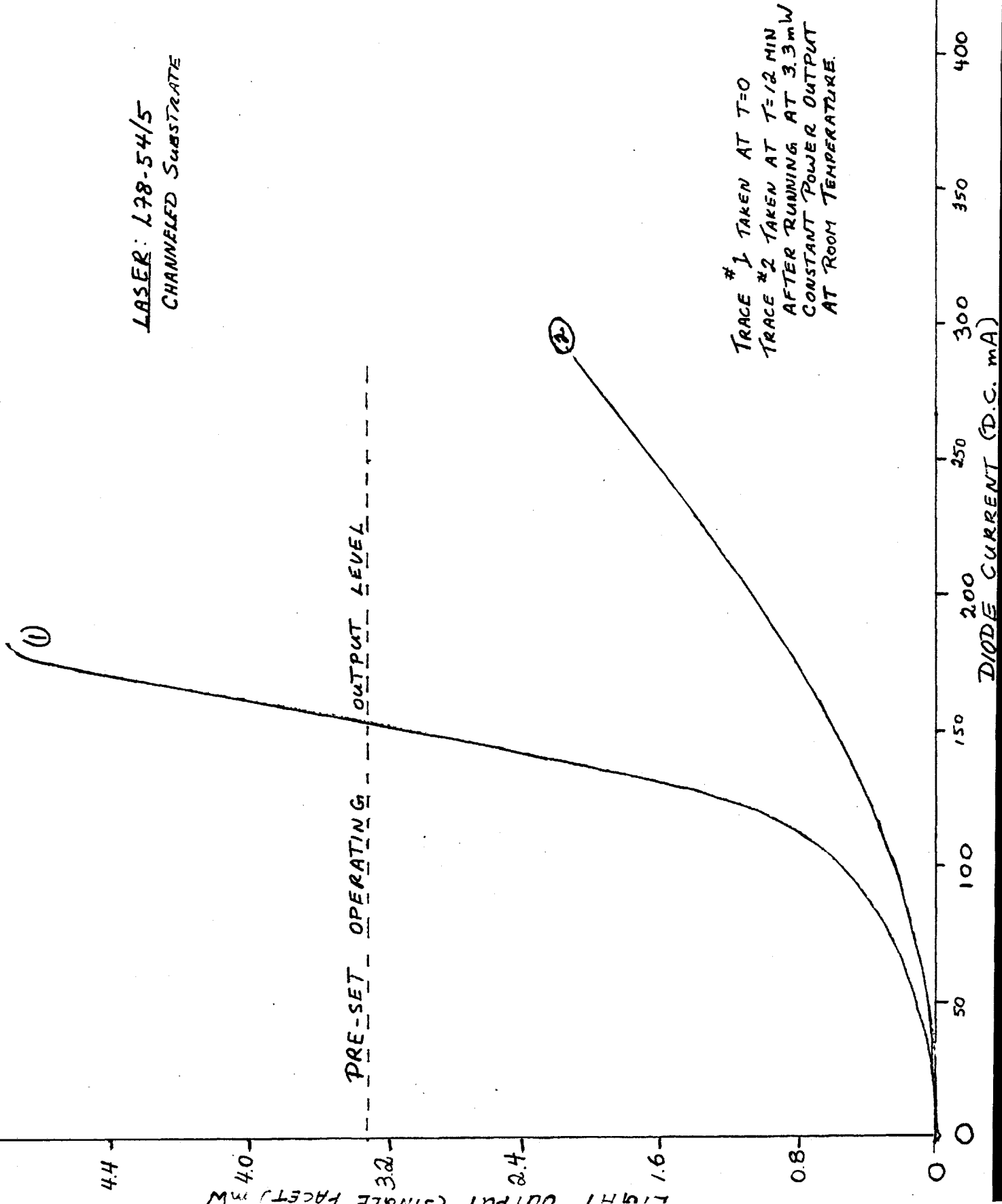
FIG. 23 Photographs of the active region of rapidly degraded lasers after failure. Photos taken at a magnification of x110 with an infra-red microscope while 5mA of D.C. current passing through device.
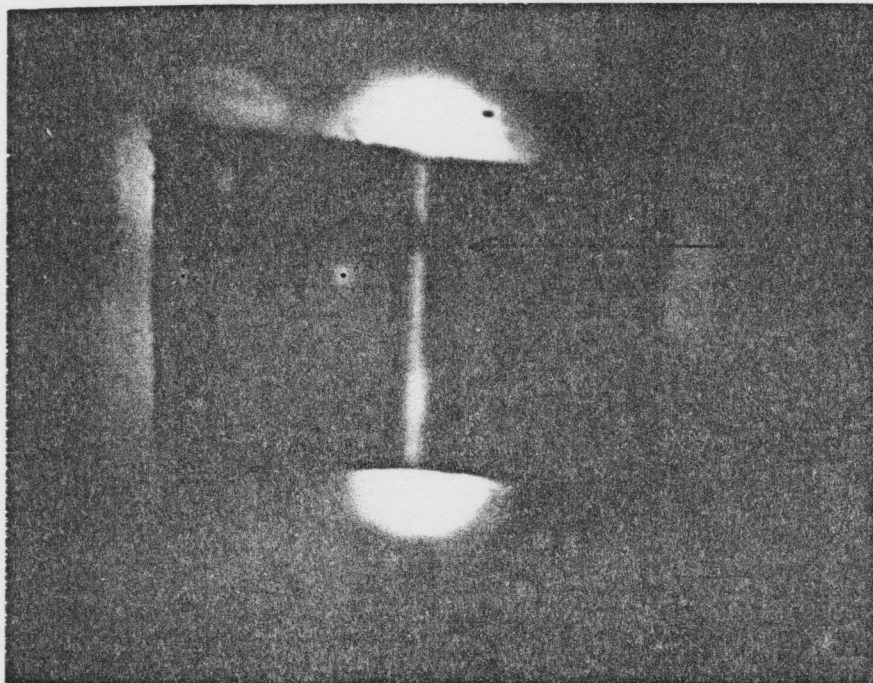
L78-55/6

Note the characteristic 100 crystalline orientation of dark region

Recall that the laser is being viewed from the top so that the semi-circles of light at each end of the laser is the scattering of the emitted radiation by the header.
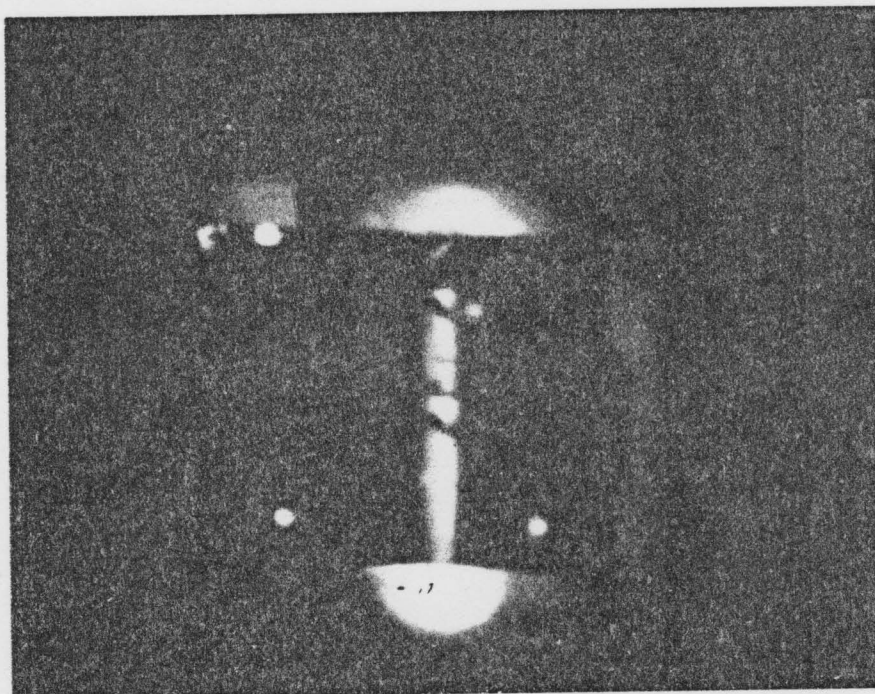
L78-54/5

This laser shows many more DLD's than the first. Note that again the direction of propagation of the DLD's are well defined. The light spots appearing at the corners are current leakage paths resulting from poor processing.

FIG. 24 Operating current required to maintain CSP laser at 4mW output at various temperatures as a function of time. The observed degradation rates were used to extract an activation energy $E_a = 0.7eV$.

TEMPERATURES GIVEN ARE THE HEAT SINK TEMPERATURES. ACTIVE REGION TEMPERATURES CALCULATED USING $\langle R \rangle = 50°C/WATT.$

$\underline{70°C}$
D.R. = 0.071 mA/hr

$\underline{50°C}$
D.R= 0.023 mA/hr

$\underline{25°C}$ ~0 mA/hr
(determined to be 0.003mA/hr by running laser at R.T. for 1000 hrs. after 70°C "failure".)
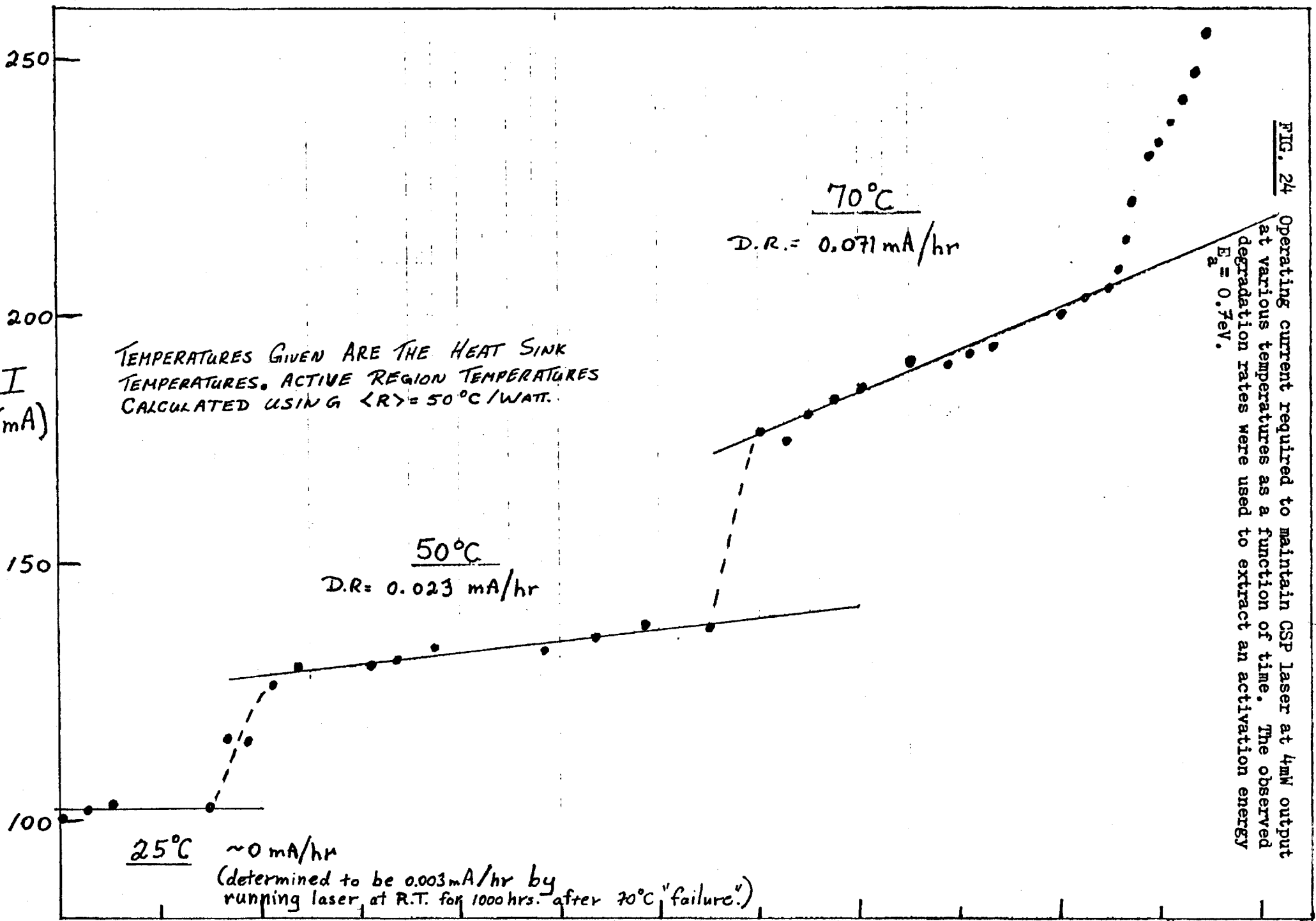
FIG. 25 L-I trace of laser operating at 50 C demonstrating the worsening of the kink with time.
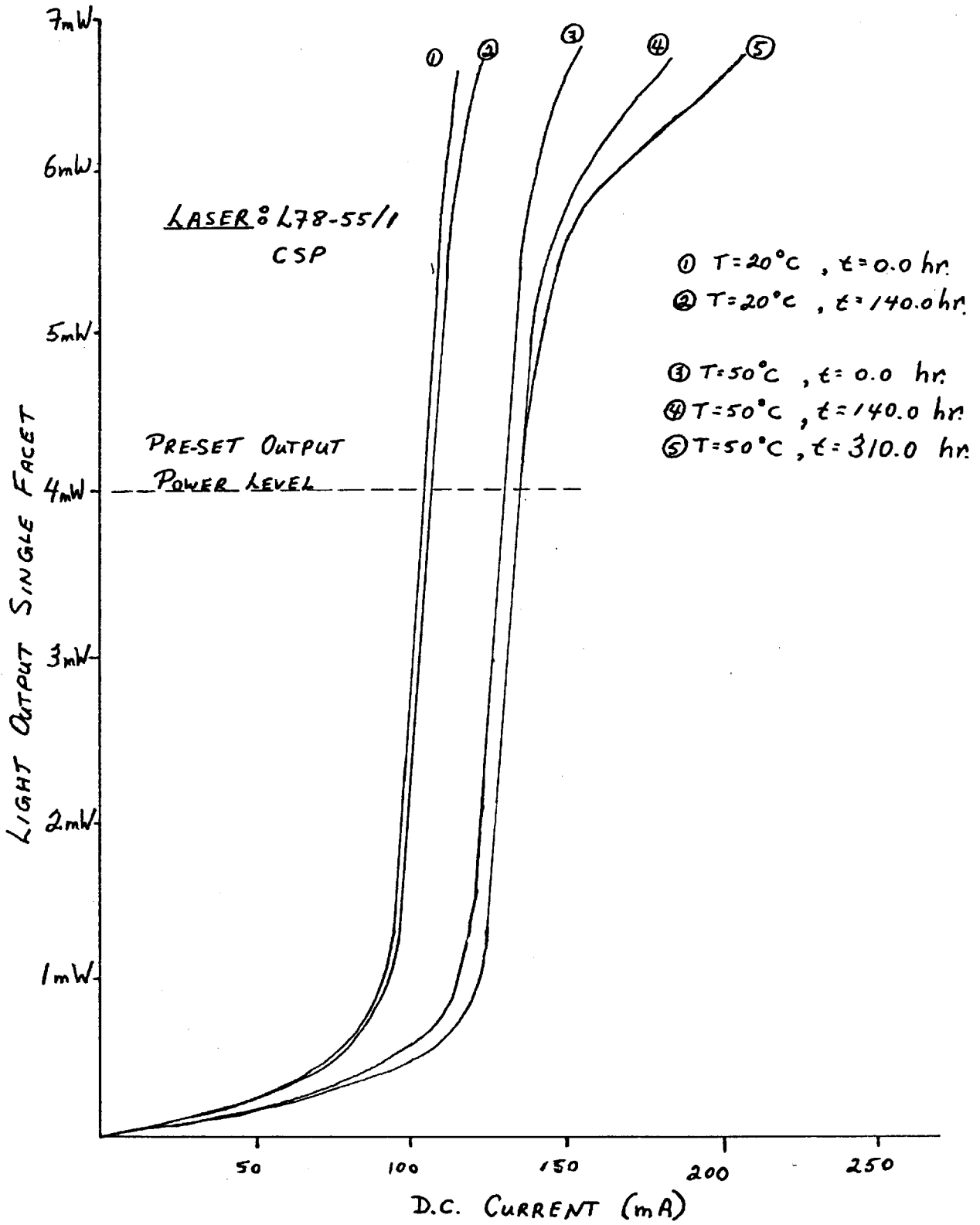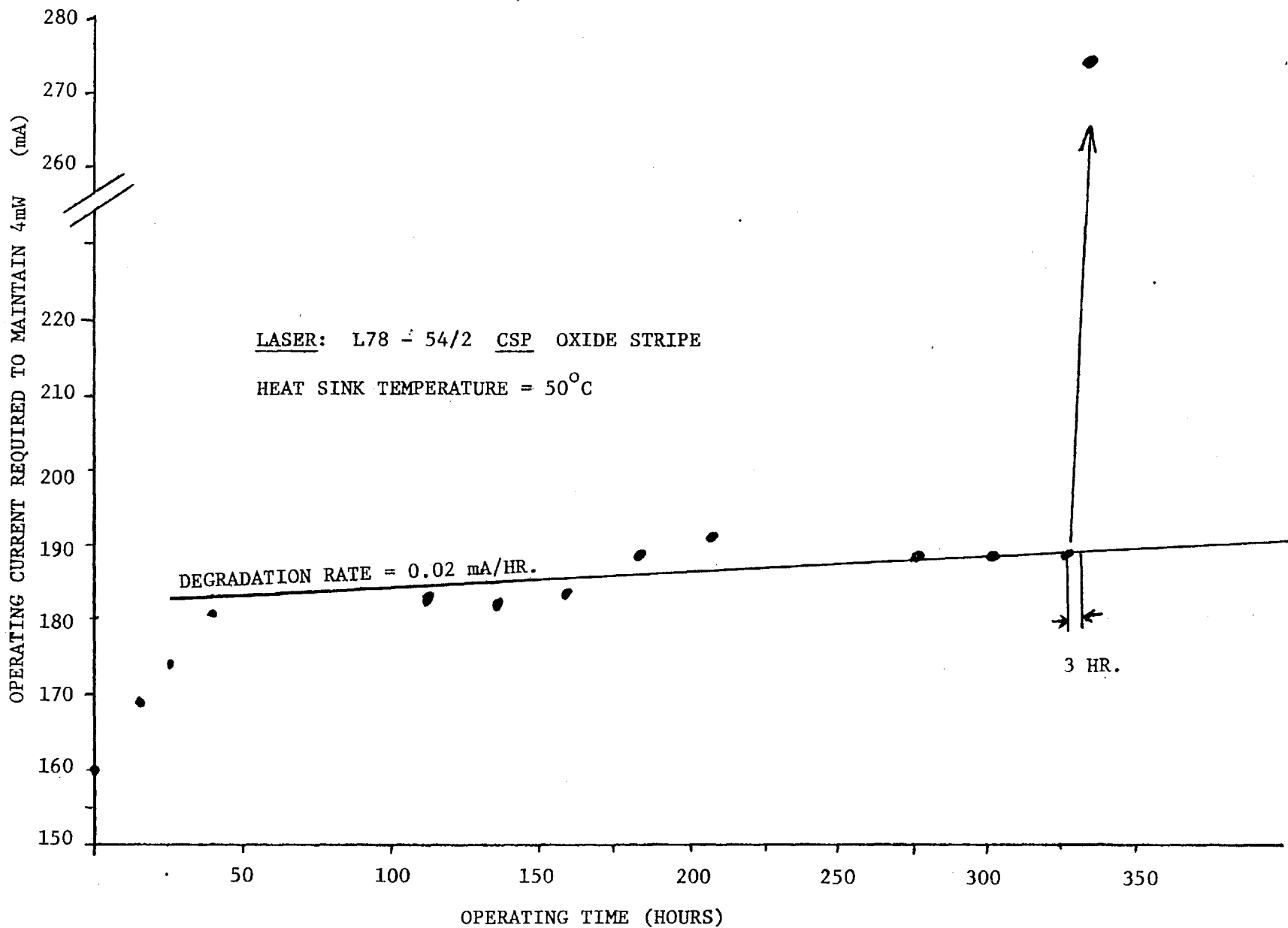
FIG. 26 Ageing behavior of an oxide stripe CSP laser showing the sudden failure mode frequently seen with this geometry.